# THE EFFECT OF ORDERING ON LOW CYCLE FATIGUE OF $Cu_3Au$

A THESIS

Presented to

The Faculty and Graduate Division

by

Kuang-Ho Chien

In Partial Fulfillment

of the Requirements for the Degree

Doctor of Philosophy

in the School of Chemical Engineering

Georgia Institute of Technology

September, 1974

THE EFFECT OF ORDERING ON LOW CYCLE FATIGUE OF $Cu_3Au$

Approved:

Edgar A. Starke, Jr., Chairman

B. G. LeFevre

R. W. Hochman

Date Approved: August 30, 1974

## ACKNOWLEDGMENTS

The author is indebted to the individuals who have contributed to the success of this work. In particular, he would like to express his sincere appreciation to his thesis advisor, Dr. Edgar A. Starke, Jr., for suggesting this problem, for his helpful guidance and continuous encouragement throughout this study. He would also like to thank Dr. R. F. Hochman and Dr. B. G. LeFevre for reviewing this work and for their constructive criticism.

The financial support of this research provided by the National Institute for Dental Research on Training Grant DE-00127 is gratefully acknowledged.

TABLE OF CONTENTS

## LIST OF ILLUSTRATIONS

LIST OF ILLUSTRATIONS (Concluded)

# LIST OF TABLES

## SUMMARY

This research was conducted to study the effect of ordering on low cycle fatigue of $Cu_3Au$. Fully ordered and disordered $Cu_3Au$ single crystals were cyclically deformed to fracture in tension-compression under strain control. Fully ordered crystals exhibit an initial rapid fatigue hardening followed by softening. Disordered crystals show continuous fatigue hardening until fracture. Fatigue hardening is interpreted by the unidirectional hardening concepts and softening by disordering.

The low cycle fatigue properties of the fully ordered and disordered crystals were investigated over a wide strain range. At very high strain amplitudes, the low cycle fatigue resistance of the disordered crystals is superior over the ordered crystals by its higher fatigue ductility coefficient. As the strain amplitude decreases, the ordered crystals become increasingly stronger than the disordered crystals by their higher fatigue ductility exponents. For both fully ordered and disordered crystals, the cyclic stress-strain curves are above the monotonic stress-strain curves. The fully ordered crystals cyclically harden much more than the disordered crystals.

For both fully ordered and disordered crystals, deformation bands develop during fatigue hardening for all strain amplitudes investigated. Fatigue cracks were observed to initiate at the intersection of slip bands and deformation bands and then propagate along the deformation band boundaries. Ordering has little effect on the fracture mode, and both fully ordered and disordered crystals show ductile fractures.

# CHAPTER I

## INTRODUCTION

Many alloys undergo atomic ordering reactions which are accompanied by some rather significant changes in their mechanical properties such as hardness, flow stresses, strain hardening rate, fatigue, creep resistance, and fracture behavior.[1] Although ordering alloys have been studied rather extensively from the standpoint of some of their mechanical properties, the effect of ordering on fatigue behavior has received relatively little attention. The data that are available are in the form of stress versus log (life) plots. Boettner et al.[2] have shown that, for $Ni_3Mn$ and Fe-Co-V in the ordered condition, deformation by superlattice dislocations causes a marked decrease in cross-slip, leading to homogeneous, planar slip and increased fatigue resistance under stress cycling conditions. Whitehead and Noble[3] studied the fatigue behavior of $Mg_3Cd$ under stress cycling conditions for both single crystal and polycrystalline specimens, in the ordered and disordered state. The results indicate that the polycrystalline material has very poor fatigue resistance for both states of order. The single crystal results show fatigue failures at lower stresses than expected for both ordered and disordered conditions. In a preliminary study of the effect of ordering on high cycle fatigue of $Cu_3Au$ single crystals, Rudolph et al.[4] have reported that the disordered crystals fractured at a resolved shear stress of 10.6 $kg/mm^2$ after about $2 \cdot 10^5$ cycles, whereas the ordered crystals fractured at 12.6 $kg/mm^2$ after about the same number of

cycles. They concluded that these stresses appeared to be true fatigue limits. No further data have been reported.

The S-N representation of fatigue resistance provides neither direct information about the mechanisms of fatigue failure, that is the mechanisms of fatigue-crack initiation and fatigue-crack propagation, nor any information about the stress-strain response of the material to cyclic deformation, that is the information of fatigue hardening/softening. An understanding of fatigue hardening/softening mechanism is basic to the interpretation of the fatigue process. Many workers have decided in favor of the strain-controlled low cycle fatigue test as the standard method for generating hardening/softening data. There are some reasons for this decision.[5] First, the test gives the flow stress versus the number of cycles (or cumulative plastic strain) directly. Second, a relationship between life and plastic strain amplitude can be obtained, and the plastic strain amplitude is the controlling parameter in the description of fatigue failure (Manson-Coffin fatigue law). Third, the test avoids cyclic creep which is often found in stress-controlled tests (especially at larger amplitudes). Fourth, the full strain amplitude can be applied on the very first cycle, whereas a "pre-hardening" period is often required before the full stress amplitude can be applied.

The main purpose of this research was to evaluate the effect of ordering on the low cycle fatigue behavior of $Cu_3Au$ single crystals in order to understand the mechanisms involved. The fatigue-crack nucleation, fatigue-crack propagation, fatigue hardening/softening, and fracture behavior of $Cu_3Au$ single crystals, in the ordered and disordered states, have been investigated under carefully selected conditions of temperature,

strain amplitude, strain rate, and crystal orientation. Single crystals were chosen so that ambiguities in the interpretation of results could be minimized. Strain-controlled, cyclic hardening/softening experiments were carried out and hysteresis loops were recorded as a function of the number of cycles. Optical and scanning electron microscopy was utilized to study the fatigue-crack nucleation and propagation, and fracture mode. Transmission electron microscopy was utilized to study the dislocation arrangements produced under cyclic loading at selected cumulative strains.

# CHAPTER II

## BACKGROUND

Copper and gold form a complete series of solid solutions with one another at all compositions. However, alloys at or near the compositions $Cu_3Au$, CuAu, and $Au_3Cu$ form an ordered arrangement of atoms when slowly cooled through the critical temperatures of 390°C, 410°C, and 250°C, respectively. X-ray superlattice lines for $Cu_3Au$ were first observed by Bain (1923). Since then hundreds of papers, both experimental and theoretical, have been devoted to an understanding of the ordering phenomena and the resulting effects on physical and mechanical properties of the alloy.

The gold and copper atoms of $Cu_3Au$, above the critical temperature of 390°C, are arranged more or less at random on the atomic sites of a face-centered cubic lattice. Below the critical temperature, the gold atoms in a perfectly ordered alloy occupy only the corner position of the unit cube and the copper atoms occupy the face-centered positions. Therefore $Cu_3Au$ has a face-centered cubic (f.c.c.) structure in the disordered state and forms an $L1_2$ structure upon ordering. The transition from random or short-range order to long-range order usually occurs at some critical temperature during cooling. The completeness of the transition or the degree of long-range order may be varied by certain thermal and/or mechanical treatments and is usually described by the LRO parameter S. Warren[6] has defined this parameter as

$$S = \frac{(R_A - X_A)}{Y_B} = \frac{(R_B - X_B)}{Y_A}$$

where $R_A$ and $R_B$ are respectively the fractions of A-sites and of B-sites occupied by the correct atoms, $X_A$ and $X_B$ are the atomic fractions of A and B atoms, $Y_A$ and $Y_B$ are the fractions of A and B lattice sites. For a stoichiometric alloy S is, therefore, zero when the alloy is perfectly random, and one when perfectly ordered.

Sachs and Weerts[7] were the first to study the striking differences in the plastic properties of $Cu_3Au$ single crystals deformed at room temperature. They found that long-range order decreased the critical resolved shear stress and increased the strain hardening rate. The changes in critical resolved shear stress as a function of degree of order in $Cu_3Au$ single crystals was also studied by Ardley.[8] In tests at temperatures near $T_c$, the ordered specimens were stronger than the disordered ones, while in quenched samples the reverse was true. A discontinuous change in strength was observed at $T_c$, where upon cooling S changes abruptly from 0 to 0.8. The strength decreased with increasing degree of order for tests carried out both at temperature and in the quenched condition.

The mechanical behavior of alloys that form superlattices has been correlated with changes in dislocation arrangements and dislocation motion with degree of order. Koehler and Seitz[9] first pointed out that an ordinary dislocation moving in a superlattice will not recreate the structure in its wake, and disorder, in the form of an antiphase boundary, will result. In order to eliminate the extra energy needed to create an antiphase boundary, dislocations in superlattices tend instead to move in groups,

connected by a strip of antiphase boundary, such that no net change in order occurs behind the dislocation group. This group, which normally consists of two unit dislocations of like sign, is called a superlattice dislocation. The equilibrium distance between the unit dislocations comprising a superlattice dislocation group is determined by an energy balance consisting of the mutual repulsive force between dislocations of like sign and the surface tension of the antiphase boundary which binds the unit dislocations together.

Superlattice dislocations in $Cu_3Au$ were first observed by Marcinkowski et al.[10] using transmission electron microscopy techniques. The superlattice dislocations consist of two pairs of partial dislocations which are held together by an antiphase boundary. The spacing between the individual partial dislocations that constitute the superlattice dislocation is a sensitive function of the degree of order and the stacking fault energy.

Theories of order strengthening have been offered by many investigators, although most of the theories have been advanced to explain only specific aspects of the phenomenon in a particular alloy system. Davies and Stoloff[1] have pointed out that since superlattice dislocations gliding in an ordered matrix create, on the average, no wrong bonds, the strength will begin to decrease as the proportion of superlattice dislocations increase. A drop in the flow stress is to be expected when a large proportion of dislocations are gliding in pairs, and the flow stress will continue to decrease with increasing order.

Davies and Stoloff[11] and Kear[12] have studied, by optical microscopy, the development of slip bands at various stages of the stress-strain curves

of single crystals of $Cu_3Au$. In the disordered condition, sharp slip bands with large offsets on the primary system are observed in the early stages of deformation, and at later stages sharp bands appear on other systems. For ordered crystals the slip lines are very fine, uniformly spaced and no cross-slip is observed until just prior to and in the region of the fracture. It has been proposed that the unit dislocations comprising a superlattice dislocation can not cross-slip individually and then be free to move since this would involve creating antiphase boundary. Also, it is unlikely that cross-slip of the associated pair can occur, because this would require the second dislocation to follow exactly in the wake of the first one. Therefore, fine slip bands may arise from blocked dislocation sources.[11]

Single crystals of f.c.c. metals generally exhibit three stages of hardening in the stress-strain curve; stage I is a region of low strain hardening rate, stage II is a linear region of high strain hardening rate, and stage III is a region of diminishing strain hardening rate. Sachs and Weerts[7] demonstrated forty years ago that crystallographic order in f.c.c. $Cu_3Au$ single crystals increased the linear strain hardening rate, $\theta_{II}$. Davies and Stoloff[11] and Kear[12] have investigated in greater detail the strain hardening behavior of $Cu_3Au$ single crystals. They observed that in the disordered condition stage I involved the discontinuous propagation of a Lüders band along the specimen; upon ordering this stage was virtually eliminated. In stage II, $\theta_{II}/G$ (where G is the shear modulus) was found to be about $2.2 \times 10^{-3}$ for the disordered state and about $4.2 \times 10^{-3}$ for the ordered condition for room temperature measurements.

Several general theories to account for the increase in strain hardening with the formation of long-range order have been proposed. Flinn[13] suggested that the refinement of the antiphase domain size by intersecting slip could result in hardening. Vidoz and Brown[14] proposed that the strain hardening of ordered alloys was the result of the creation of antiphase boundary ribbons behind jogs in superlattice dislocations created by intersecting slip. Kear[12] has proposed that the flow stress of ordered $Cu_3Au$, $\tau$, is given by $\tau = \tau_F + \tau_C$, where $\tau_F$ is the frictional stress and $\tau_C$ is the critical stress to bow out glissile edge segments of the loop between the jogs formed when the screw segments undergo cross-slip. $\tau_C$, which makes the major contribution to the strain hardening, is (Gb/L) where b is the Burgers vector and L is the average width of the glissile edge segments of the dislocation loop. Davies and Stoloff[11,15] suggested that the strain hardening in ordered $Cu_3Au$ was due to an exhaustion type of hardening. As a superlattice dislocation loop expands from a source, there is a finite probability that the screw component will cross-slip onto another (111) plane so that the antiphase boundary can lower its energy on a (100) plane. If cross-slip occurs a strong barrier will be created, for to move further either of the dislocations comprising the barrier would create antiphase boundary; this is energetically unfavorable, so that the unit dislocations are effectively sessile. Thus other dislocations from the same source will not be able to move large distances before being held up at the barrier. For further slip to take place, sources on neighboring planes will have to operate.

Recently, Czernichow and Marcinkowski[16] conducted a compression test for single crystals of a fully ordered $Cu_3Au$ alloy at room temperature.

Transmission electron microscopy observations showed a very high density of superlattice screw dislocations which had cross-slipped onto (100) type planes. They suggested that it is this large density of cross-slipped superlattice dislocations which is believed responsible for the high rate of strain hardening observed in ordered $Cu_3Au$ alloys.

The effect of ordering on the twinning modes of $Cu_3Au$ single crystals has been recently studied by Chakrabortty[17] and Starke. It is found that ordering changes the twinning process in two ways, viz, by imposing crystallographic restrictions and by changing the stacking fault energy. For disordered and partially ordered crystals, the shear stress required for twinning increases with the degree of order due to crystallographic restrictions imposed by the order. However, the twinning stress required for the fully ordered crystals was comparatively low because ordering lowered the stacking fault energy and did not impose any crystallographic restrictions for its particular twinning mode.

To further understand the effect of ordering on the mechanical properties of $Cu_3Au$ alloy, a detailed evaluation of the effect of ordering on its fracture and fatigue behavior is essential. Since no such data have been reported, the present study was initiated.

# CHAPTER III

# EXPERIMENTAL PROCEDURES

## 3.1 Growth of Single Crystals

The $Cu_3Au$ alloy for this work was kindly provided by J. F. Jelenko & Co. The alloy was made at a nomial composition of 50.85 weight percent gold and 49.15 weight percent copper. The alloy was melted in an induction furnace and poured into a 12.7 mm diameter oil coated steel mold. The alloy was remelted as a further assurance of homogeneity.

This alloy was homogenized in an evacuated Vycor tube for one week at 880°C. After the homogenization it was swaged into rods from which single crystals of about 4 mm diameter were grown in a vacuum of $10^{-4}$ torr by a modified Bridgman technique using high purity graphite molds. The orientation of the crystals, which is given in Figure 1, was controlled by using seed crystals and was determined by the Laue back reflection X-ray technique. The orientation was chosen to give single slip. X-ray lattice parameter determination of several crystals gave lattice parameters of from 3.7514 Å to 3.7543 Å, which is the range of the lattice parameters for stoichiometric $Cu_3Au$ reported in the literature.[18,19]

## 3.2 Heat Treatments and Order Determination

The crystals were annealed in evacuated Vycor tubes in the following way:

(i) Disordered alloy--annealed at 880°C for 24 hours, furnace cooled to 500°C and quenched into ice water.

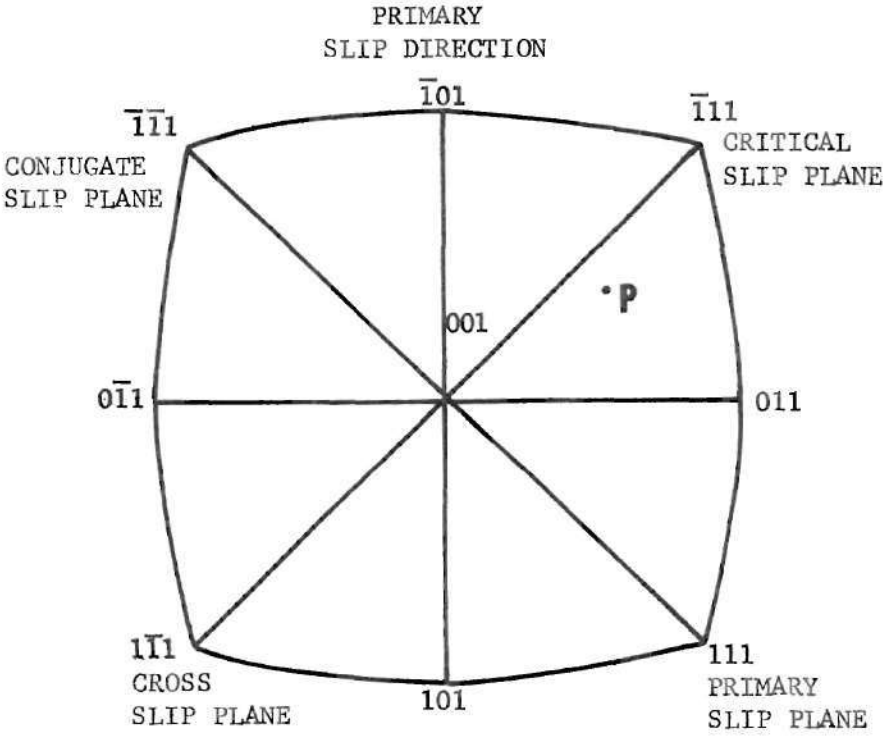


Figure 1. Orientation of $Cu_3Au$ Single Crystals

(ii) Fully ordered alloy--annealed at 880°C for 24 hours, followed by 72 hours at 350°C, and cooled 10°C/day to 150°C, and then furnace cooled to room temperature. This treatment had been previously shown to produce a long-range order parameter close to one for $Cu_3Au$.[20]

Small disks parallel to (110) planes, to be used to evaluate the degree of long-range order, were cut from the single crystals and electropolished in a solution consisting of 20 gm chromic acid, 135 ml glacial acetic acid, and 7 ml of distilled water to remove any deformed surface layer. The (110) and (220) diffraction peaks were then measured with a diffractometer using Cu-$K_\alpha$ radiation. The long-range order parameters, S, were determined from integrated intensities as described by Chipman.[21] Results showed that S=0 for the disordered alloy and S=1 for the fully ordered alloy within experimental accuracy of $\pm$ 0.10.

## 3.3 Preparation of Specimens

Specimens were cut from the single crystals using a Servomet spark cutter. Tensile specimens were prepared from the 4 mm diameter single crystal rods. A gage section, about 14 mm long, was reduced to about 3 mm diameter by spark machining. Finishing was done by electropolishing to remove any deformed surface layer.

Low cycle fatigue specimens were prepared from the 4 mm diameter single crystal rods by spark machining. Since longitudinal strain was going to be measured, straight gage sections were essential. To prevent buckling, two different types of specimens were found necessary to permit determination of fatigue properties over a wide strain range. A gage section 2.5 mm diameter and 3.75 mm long was used for short life high

strain (in excess of ± 6.58 percent total shear strain amplitude) specimen. In the intermediate life range (less than ± 6.58 percent total shear strain amplitude), a gage section of 2.5 mm diameter and 5 mm long was used to allow more accurate strain control. Finishing was accomplished by electropolishing to remove any deformed surface layer.

## 3.4 Low Cycle Fatigue Testing

All the low cycle fatigue testings were conducted in a 10,000 kg capacity Instron Testing machine (Model TT-DM-L) equipped with reverse stress modification. Gripping of the specimens proved to be one of the most difficult aspects of the present investigation. After many trials, the technique found to be most successful is as follows. One end of the specimen was mechanically fixed to a specimen holder, which through an adapter was connected to the top of the Instron machine. To obtain a good alignment, the other end of the specimen was attached by a specimen holder and then mounted in a Wood's metal grip which was adapted to the movable crosshead. The distance between the two specimen holders was set very close to the gage length of the specimen. The extension was measured and controlled by an Instron strain extensometer. To prevent any bending of the specimen, the extensometer was not directly attached to the specimen. Instead, the displacement between the two specimen holders was measured. The specimens were cyclically strained by first imposing a tensile strain, and then an equal compressive strain. Cycles were subsequently repeated by the combination of the manual operation and the Instron automatic extension cycling device. The automatic cycling capability of the Instron machine did not satisfy the test conditions when the specimens were

experiencing rapid cyclic hardening or softening. During this period manual operation was employed. When the rate of cyclic hardening or softening was moderate, the Instron automatic extension cycling device was used. All tests were conducted in air, at room temperature, and at a crosshead speed of 0.1 cm per minute (strain rate approximately $3 \times 10^{-3}$ per second). The test frequency was approximately 1 cycle per minute. The information was obtained by the continual plotting of the hysteresis loops from the Instron recorder. Tensile tests were made on the same machine at a crosshead speed of 0.1 cm/min.

### 3.5 Surface Damage and Fractographic Observations

Operating slip planes were determined through the study of the slip pattern around the circumference of the specimens and measuring the angles between the tangents to the slip traces and the specimen axis. Fatigue-crack nucleation and propagation were observed from the circumference of the specimens during the tests. The fatigue-crack mentioned here was defined as the smallest crack first visible to the naked eye. This is not to be confused with the micro-crack mentioned elsewhere. Fracture surfaces were studied by scanning electron microscopy. Button-type specimens used for scanning electron microscopy were cut from the fracture surfaces of the low cycle fatigue specimens.

### 3.6 Transmission Electron Microscopy

Disks were sectioned with the primary slip plane (111) approximately parallel to the surface from the fatigued specimens. Specimens for transmission electron microscopy were polished by conventional methods.[22]

Electrolytic jet polishing was carried out using an electrolyte solution of 110 ml of glacial acetic acid and 10 ml of perchloric acid. Final polishing was accomplished with a solution of 20 gm chromic acid, 7 ml distilled water, and 135 ml glacial acetic acid.[23] The specimen was under continuous observation during final polishing. When a hole appeared in the thinned area, the specimen was taken out and cleaned thoroughly in water and alcohol. The foils were then examined in a Siemens Elmiskop 1A electron microscope operating at 125KV.

# CHAPTER IV

# RESULTS

## 4.1 Uniaxial Tension Test

Figure 2 shows the tensile stress-strain and resolved shear stress-shear strain curves for the alloy used in this investigation in fully ordered and disordered state.

The disordered crystal shows the characteristic three stages of hardening for an f.c.c. crystal. In stage I plastic deformation occurred in a discontinuous manner, and by the propagation of a Lüders band in the primary system as pointed out by previous workers.[8,12] The band was initiated at one end of the specimen near the grips, accompanied by a drop in stress, and required all of stage I to propagate over the whole gage length. In stage II no significant change was observed, but the transition from stage II to stage III was marked by the appearance of a new Lüders band in the conjugate system.

The stress-strain curve for the fully ordered crystal is unusual for an f.c.c. crystal. Stage I in the classic sense of easy glide has not been observed. In stage II, strong, linear strain-hardening was observed, and slip occurred mainly on the primary system. The uniaxial tensile test result is consistent with that reported by Sachs and Weerts.[7] Long-range order decreased the critical resolved shear stress and increased the strain hardening rate.

The tensile tests were necessary, since the tensile stress-strain

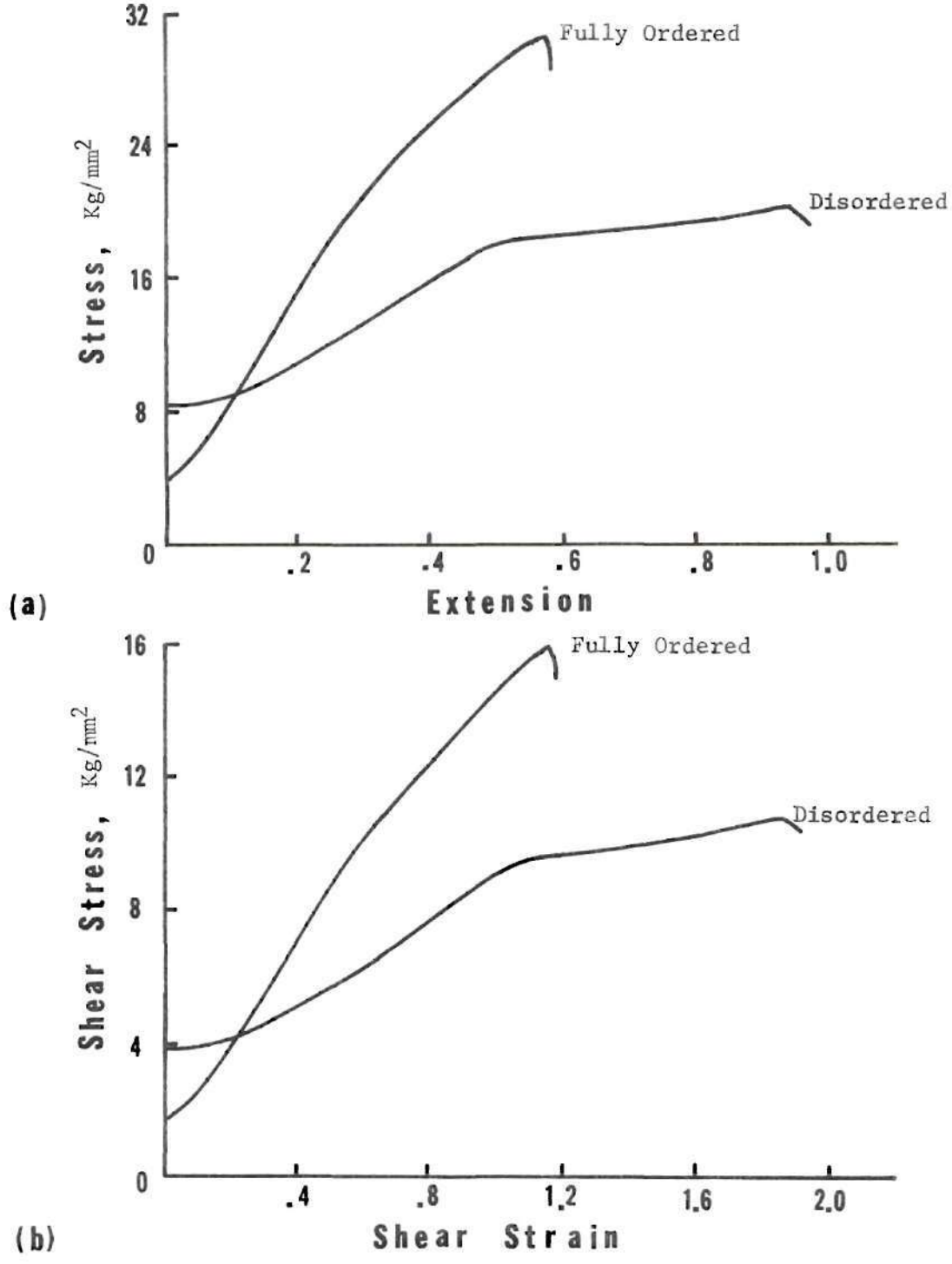


Figure 2. (a) Tensile Stress-Strain, and (b) Resolved Shear Stress-Shear Strain Curves of $Cu_3Au$ Single Crystals Deformed at Room Temperature

curves were used to compare with the cyclic stress-strain curves to determine cyclic hardening or softening. In addition, the true fracture strain plays a significant role in low cycle fatigue properties.

## 4.2 Fatigue Hardening/Softening

Fatigue specimens cycled under strain control were monitored by recording hysteresis loops showing the stress-strain response at different parts of the life. Figures 3 and 4 show respectively the typical cyclic stress-strain response of a fully ordered and a disordered specimen tested at a total shear strain amplitude of ± 10.92%. The shape of the hysteresis loops are roughly symmetric about the tip to tip axis in the early part of the fatigue life. However, in the later part of the fatigue life, after a fatigue-crack developed in a specimen, an inflection point in the compressive half of the hysteresis loop can be observed. The strain at any stress level can be separated into elastic and plastic components. In a qualitative assessment, the deformation indicated by the cyclic hysteresis loops in Figures 3 and 4 are predominantly plastic. The plastic strain per cycle is large. This is the characteristic cyclic deformation of ductile materials. The area enclosed by the hysteresis loop indicates the energy dissipated per cycle.

The peak compressive stress is slightly larger than the peak tensile stress for equal strain amplitude. The difference was greater during the early stage of the fatigue life, when the material was experiencing rapid fatigue hardening, and it became smaller as the number of cycles increased. Fully ordered crystals showed a larger difference than the disordered crystals, and the difference increased with increasing strain amplitude.

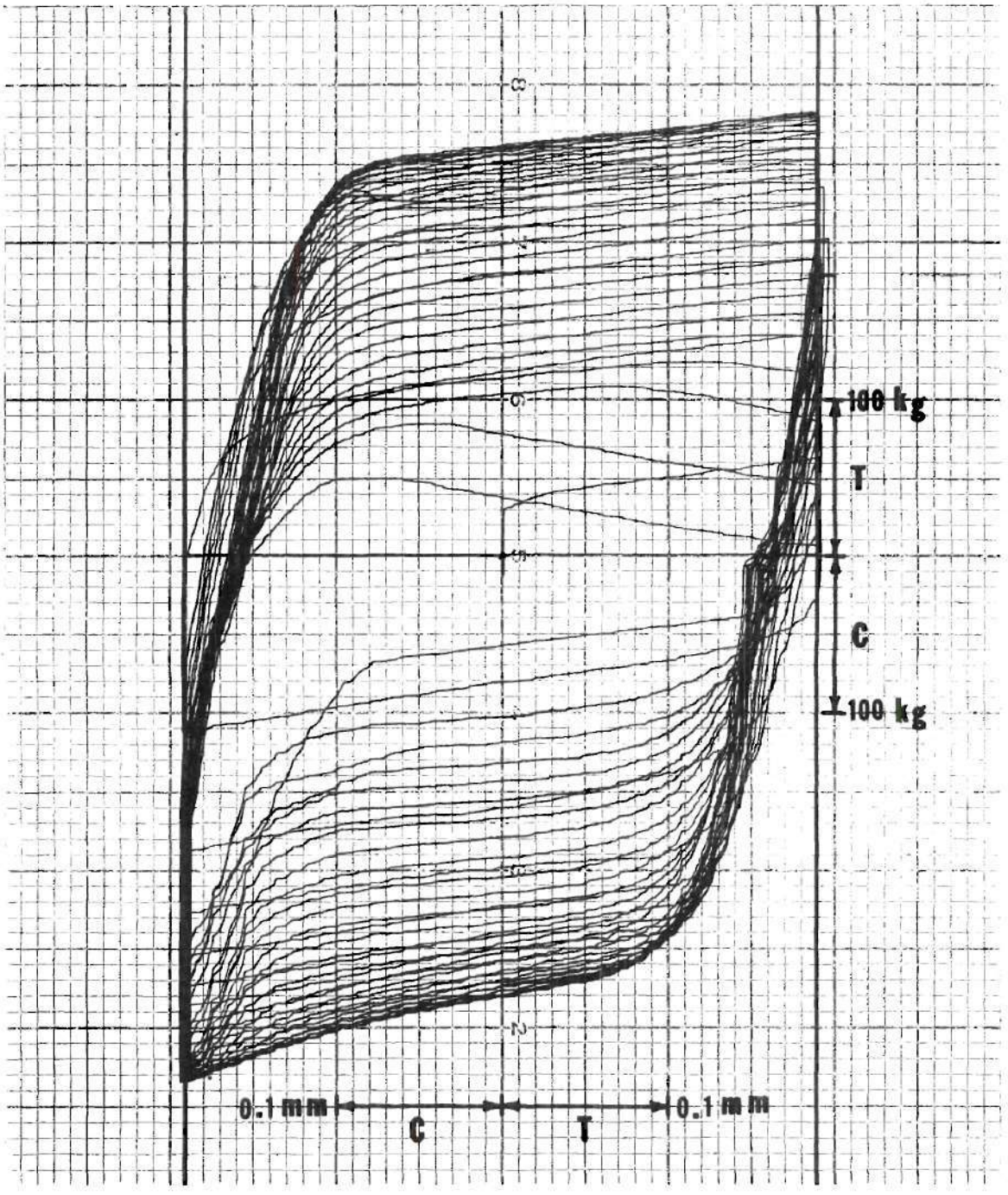


Figure 3. Hysteresis Loops for a Fully Ordered Crystal Cycled at a Total Shear Strain Amplitude of ± 10.92%

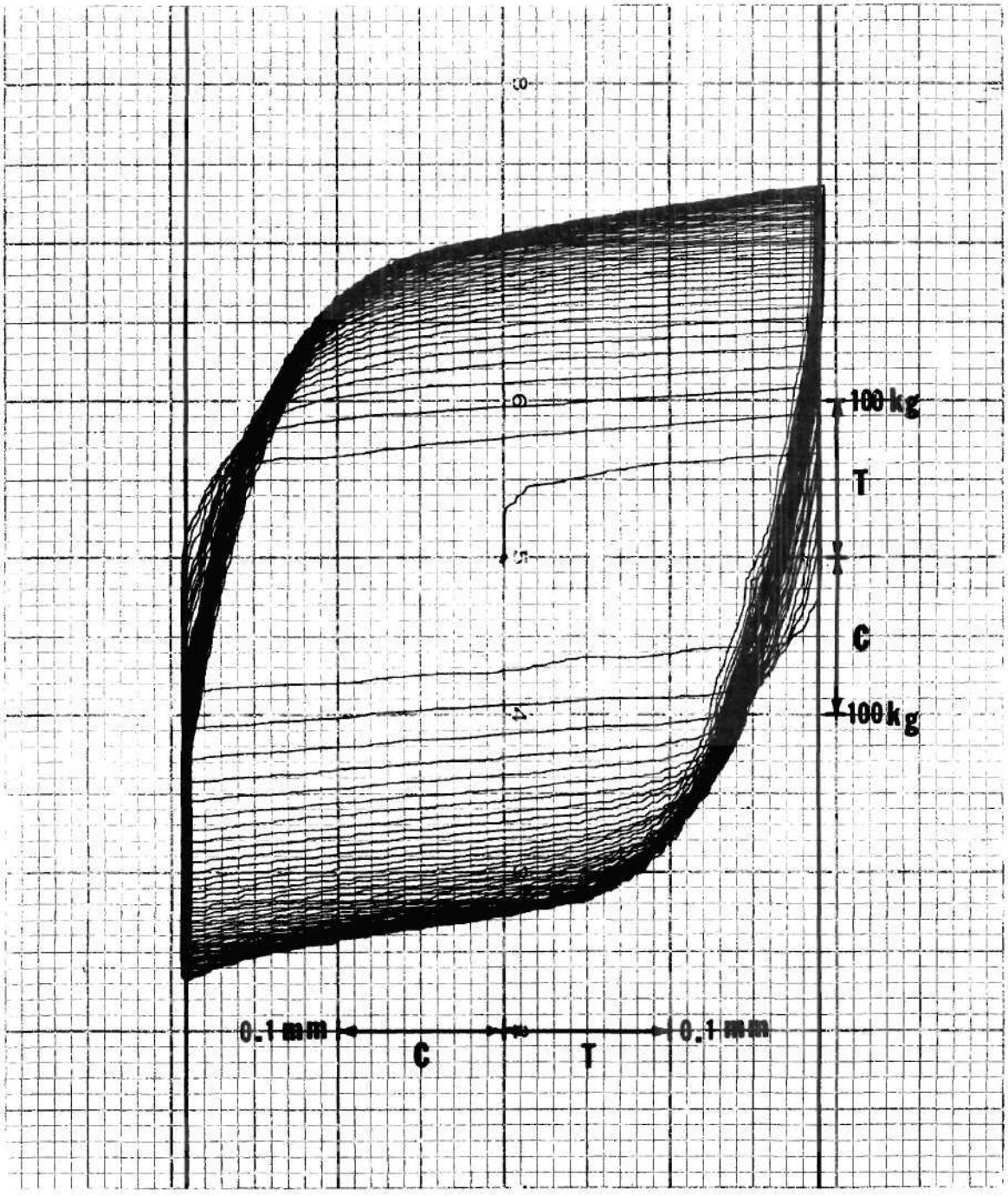


Figure 4. Hysteresis Loops for a Disordered Crystal Cycled at a Total Shear Strain Amplitude of ± 10.92%

The most important feature of the cyclic stress-strain response, however, is that it is unstable with respect to continued cycling; both the resistance to plastic deformation and the cyclic hysteresis undergo marked changes. In Figure 3, for instance, the fully ordered crystals show an initial rapid cyclic strain hardening followed by cyclic strain softening. However, the disordered crystals as shown in Figure 4 show continuous cyclic strain hardening. This can be seen more clearly in Figures 5 and 6, which are plots of the mean peak resolved shear stress (the arithmetic average of peak resolved shear stresses at the end of tensile and compressive half cycles) versus, N, the number of cycles.

The effect of strain amplitude was investigated by varying the total shear strain amplitude between $\Delta\gamma_t/2 = \pm 1.65\%$ and $\Delta\gamma_t/2 = \pm 10.92\%$ (total strain amplitude between $\Delta\epsilon_t/2 = \pm 0.75\%$ and $\Delta\epsilon_t/2 = \pm 5.0\%$). Stresses and strains are resolved in the (111) $[\bar{1}01]$ primary slip system, since the slip trace analysis indicates that crystals deformed by slip in this system.

The fatigue hardening/softening behavior for fully ordered crystals is summarized in Figure 5. At the lower shear strain amplitude (± 2.2% and ± 1.65%) tests, the curves consist of three well defined stages; an initial stage of rapid hardening followed by a stage of softening, and a final stage of very slow softening. At the intermediate shear strain amplitude (± 5.23%, ± 4.4%, and ± 3.3%) tests, the curves consist of two stages; an initial stage of rapid hardening followed by a stage of softening. For the higher shear strain amplitude (± 10.92%, ± 7.8%, and ± 6.58%) tests, the curves exhibit only one stage; the rapid hardening stage. It should be noted that hardening or softening occurred by a gradual increase or decrease in both the tension and compression stress. The rapid cyclic

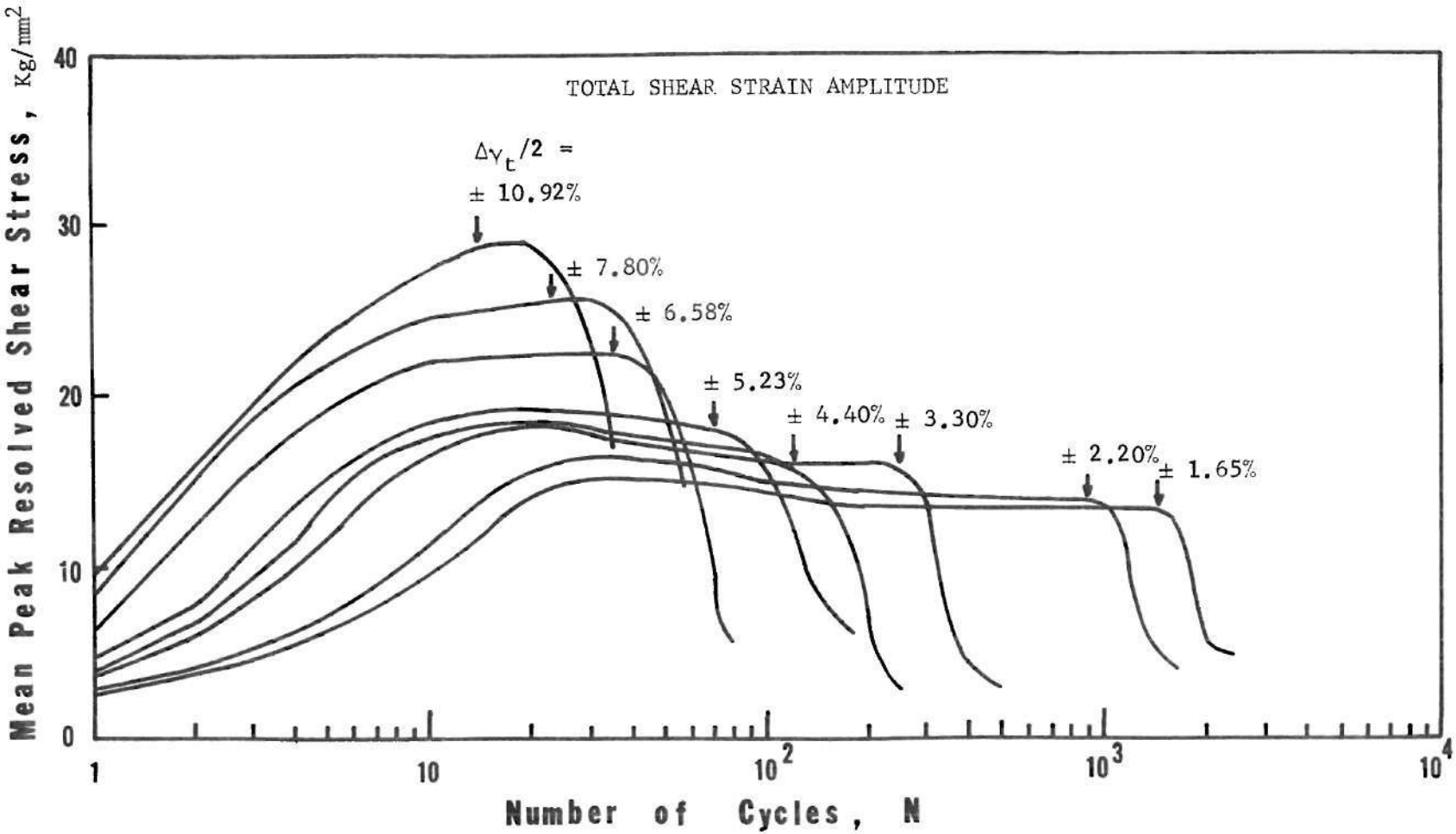


Figure 5. Fatigue Hardening/Softening Curves for Fully Ordered Crystals

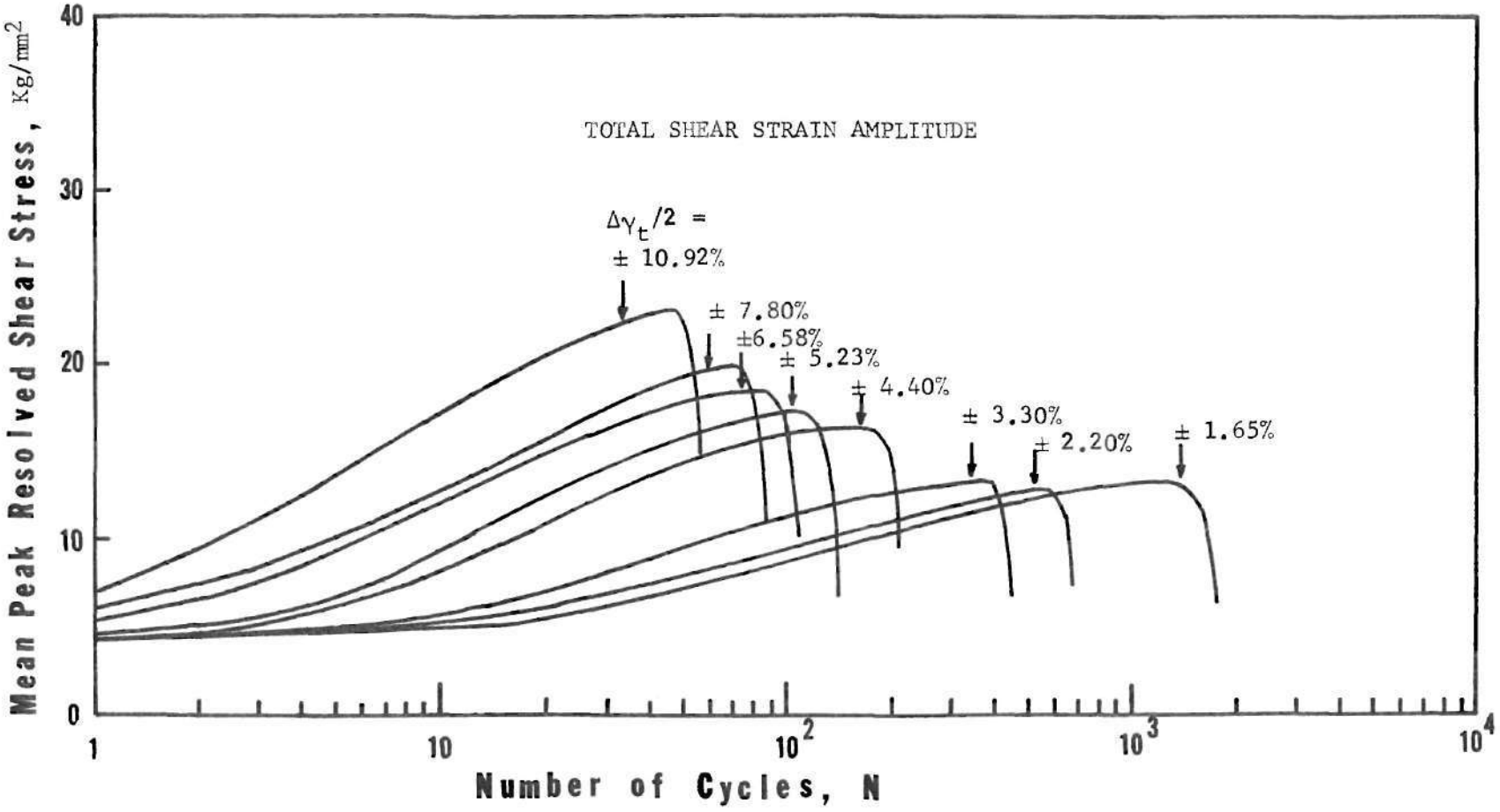


Figure 6. Fatigue Hardening Curves for Disordered Crystals

softening shown in all curves just prior to fracture is due to the propagation of a fatigue-crack, and should not be confused with the cyclic hardening/softening behavior of the materials. In Figures 5 and 6, an arrow is indicated on each curve at the point where the fatigue-crack was first observed by naked eye. It can be seen that for the higher shear strain amplitude tests, cracks were observed prior to peak hardening, whereas at the lower shear strain amplitude tests, the cracks formed only well after the peak stress. In all cases the cyclic hardening and softening rate increased with increasing strain amplitude, and at larger shear strain amplitude, a larger fraction of life was spent in fatigue hardening.

Figure 6 summarizes the fatigue hardening/softening behavior for disordered crystals. Cyclic hardening occurred in all cases. The hardening rate is low when compared to those in the initial stage of fully ordered crystals. The cyclic hardening rate increased with increasing strain amplitude. For the lower shear strain amplitude ($\pm$ 3.3%, $\pm$ 2.2%, and $\pm$ 1.65%) tests, the plastic deformation occurred in a discontinuous manner in the first few cycles and then became smooth. This is similar to the behavior in the initial stage of the tensile test for a disordered crystal. In all cases, the cyclic hardening continued, though the rate of hardening decreased as the number of cycles increased, until fatigue cracking occurred. Once the crack or cracks were initiated, the tensile stress began to decrease, but the compressive stress continued to increase for some cycles. This resulted in a slight increase in the mean peak resolved shear stress after the cracks were observed, as can be seen in Figure 6. The final stage of fatigue life was occupied by the rapid softening due to fatigue-crack propagation.

The fatigue hardening/softening curves can also be expressed as peak stress versus total cumulative plastic strain. If the strain is summed without regard to sign, the total plastic strain after N cycles is $2\Delta\epsilon_p \cdot N$, where $\Delta\epsilon_p$ is the tensile plastic strain range. In Figures 7 and 8, typical results for fully ordered and disordered crystals are plotted as the mean peak resolved shear stress versus cumulative plastic shear strain. Here, the total plastic shear strain after N cycles is $2\Delta\gamma_p N$ where $\Delta\gamma_p$ is the plastic shear strain range taken from half-life data.

## 4.3 Low Cycle Fatigue Behavior

A summary of the low cycle fatigue data generated in this study is presented in Table 1 and Table 2 for fully ordered and disordered crystals, respectively. In the present investigation, since a steady state or saturation condition was never obtained, the half-life data were used. The reported fatigue lives, $N_f$, of the specimens are the number of strain cycles required for total separation, whereas $N_0$ represents the number of cycles to the point where fatigue cracks were first observed by naked eye, and $N_p$ represents the number of cycles spent for fatigue-crack propagation. From Tables 1 and 2, several important low cycle fatigue properties can be generated.

The low cycle fatigue properties can be best understood by plotting the plastic strain amplitude, $\Delta\epsilon_p/2$, versus the reversals to failure, $2N_f$. Figure 9 is that of a plot for the fully ordered crystals. The straight line was obtained by using a computer program for least-squares fit. The slope, - 0.48, is the fatigue ductility exponent, c. The ordinate intercept, 0.33, is the fatigue ductility coefficient, $\epsilon_f'$. Therefore, the

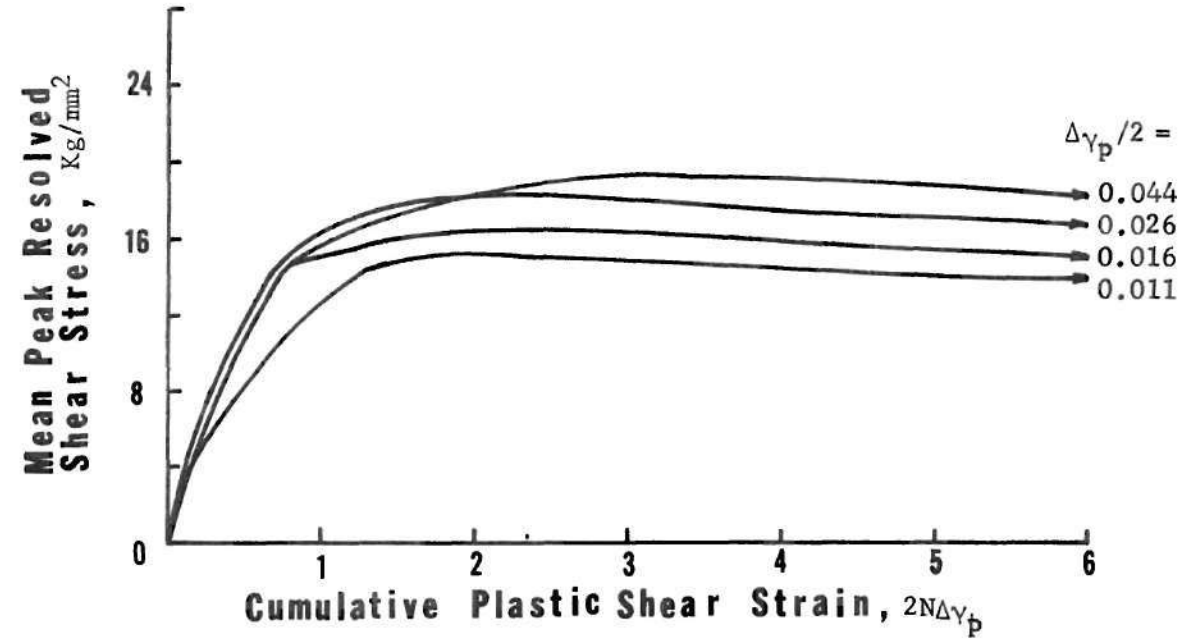


Figure 7. Fatigue Hardening/Softening Curves for Fully Ordered Crystals

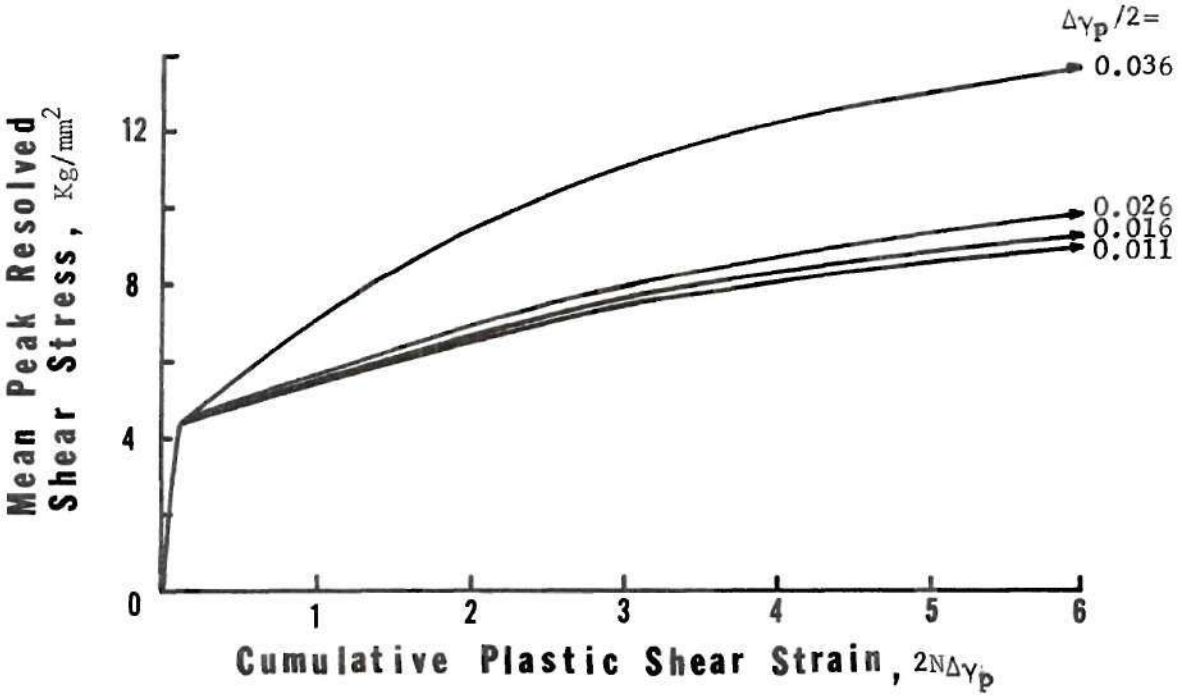


Figure 8. Fatigue Hardening Curves for Disordered Crystals

TABLE 1. Summary of Room Temperature Low Cycle Fatigue Test Data for Fully Ordered Crystals

| Specimen No. | Frequency cycles/min. | Total Strain Ampli. $\Delta\varepsilon_t/2.\%$ | Total Shear Strain Ampli. $\Delta\gamma_t/2.\%$ | Half Life Data | | | | | | Fatigue Life | | | |
|---|---|---|---|---|---|---|---|---|---|---|---|---|---|
| | | | | Stress Ampli. $\Delta\sigma/2.$ Kg/mm | Shear Stress Ampli. $\Delta\tau/2.$ Kg/mm | Plastic Strain Ampli. $\Delta\varepsilon_p/2.\%$ | Plastic Shear Strain Ampli. $\Delta\gamma_p/2.\%$ | Elastic Strain Ampli. $\Delta\varepsilon_e/2.\%$ | Elastic Shear Strain Ampli. $\Delta\gamma_e/2.\%$ | $N_o$* Cycles | $N_f$** Cycles | $N_p$*** Cycles | $N_o/N_f$ |
| 4-4 | 1 | 5.00 | 10.92 | 62.75 | 29.07 | 4.47 | 9.76 | 0.53 | 1.16 | 14 | 36 | 22 | 0.39 |
| 3-4 | 1 | 3.56 | 7.80 | 55.79 | 25.69 | 3.07 | 6.73 | 0.49 | 1.07 | 23 | 57 | 34 | 0.40 |
| 3-5 | 1 | 3.00 | 6.58 | 48.31 | 22.17 | 2.55 | 5.60 | 0.45 | 0.98 | 35 | 81 | 46 | 0.42 |
| 3-3 | 1 | 2.38 | 5.23 | 38.10 | 17.48 | 2.00 | 4.39 | 0.38 | 0.84 | 80 | 180 | 100 | 0.44 |
| 3-2 | 1 | 2.00 | 4.40 | 33.40 | 15.30 | 1.65 | 3.63 | 0.35 | 0.77 | 120 | 263 | 143 | 0.46 |
| 4-3 | 1.5 | 1.50 | 3.30 | 34.58 | 15.76 | 1.17 | 2.57 | 0.33 | 0.73 | 250 | 496 | 246 | 0.50 |
| 4-1 | 2 | 1.00 | 2.20 | 30.78 | 14.00 | 0.73 | 1.61 | 0.27 | 0.59 | 900 | 1700 | 800 | 0.53 |
| 7-5 | 3 | 0.75 | 1.65 | 29.85 | 13.56 | 0.51 | 1.12 | 0.24 | 0.53 | 1460 | 2400 | 940 | 0.61 |

*$N_o$ = number of cycles to the point where fatigue-cracks were first observed under the naked eye

**$N_f$ = number of cycles to failure

***$N_p = N_f - N_o$

TABLE 2. Summary of Room Temperature Low Cycle Fatigue Test Data for Disordered Crystals

| Specimen No. | Frequency Cycles/min. | Total Strain Ampli. $\Delta\varepsilon_t/2.\%$ | Total Shear Strain Ampli. $\Delta\gamma_t/2.\%$ | Half Life Data | | | | | | Fatigue Life | | | |
|---|---|---|---|---|---|---|---|---|---|---|---|---|---|
| | | | | Stress Ampli. $\Delta\sigma/2._2$ Kg/mm | Shear Stress Ampli. $\Delta\tau/2._2$ Kg/mm | Plastic Strain Ampli. $\Delta\varepsilon_p/2.\%$ | Plastic Shear Strain Ampli. $\Delta\gamma_p/2.\%$ | Elastic Strain Ampli. $\Delta\varepsilon_e/2.\%$ | Elastic Shear Strain Ampli. $\Delta\gamma_e/2.\%$ | $N_o$* Cycles | $N_f$** Cycles | $N_p$*** Cycles | $N_o/N_f$ |
| 6-5 | 1 | 5.00 | 10.92 | 47.00 | 21.76 | 4.44 | 9.70 | 0.56 | 1.22 | 33 | 56 | 23 | 0.59 |
| 1-4 | 1 | 3.56 | 7.80 | 41.15 | 18.95 | 3.05 | 6.69 | 0.51 | 1.11 | 60 | 89 | 29 | 0.67 |
| 6-4 | 1 | 3.00 | 6.58 | 39.00 | 17.90 | 2.54 | 5.58 | 0.46 | 1.00 | 75 | 115 | 40 | 0.65 |
| 2-3 | 1 | 2.38 | 5.23 | 36.26 | 16.60 | 2.00 | 4.39 | 0.38 | 0.84 | 103 | 144 | 41 | 0.72 |
| 2-2 | 1 | 2.00 | 4.40 | 35.00 | 16.00 | 1.64 | 3.61 | 0.36 | 0.79 | 165 | 213 | 48 | 0.77 |
| 5-3 | 1.5 | 1.50 | 3.30 | 28.00 | 12.77 | 1.22 | 2.68 | 0.28 | 0.62 | 340 | 448 | 108 | 0.75 |
| 5-2 | 2 | 1.00 | 2.20 | 26.70 | 12.10 | 0.76 | 1.67 | 0.24 | 0.53 | 510 | 676 | 166 | 0.75 |
| 5-4 | 3 | 0.75 | 1.65 | 28.93 | 13.14 | 0.57 | 1.25 | 0.18 | 0.40 | 1400 | 1800 | 400 | 0.78 |

*$N_o$ = number of cycles to the point where fatigue-cracks were first observed by the naked eye.

**$N_f$ = number of cycles to failure

***$N_p = N_f - N_o$

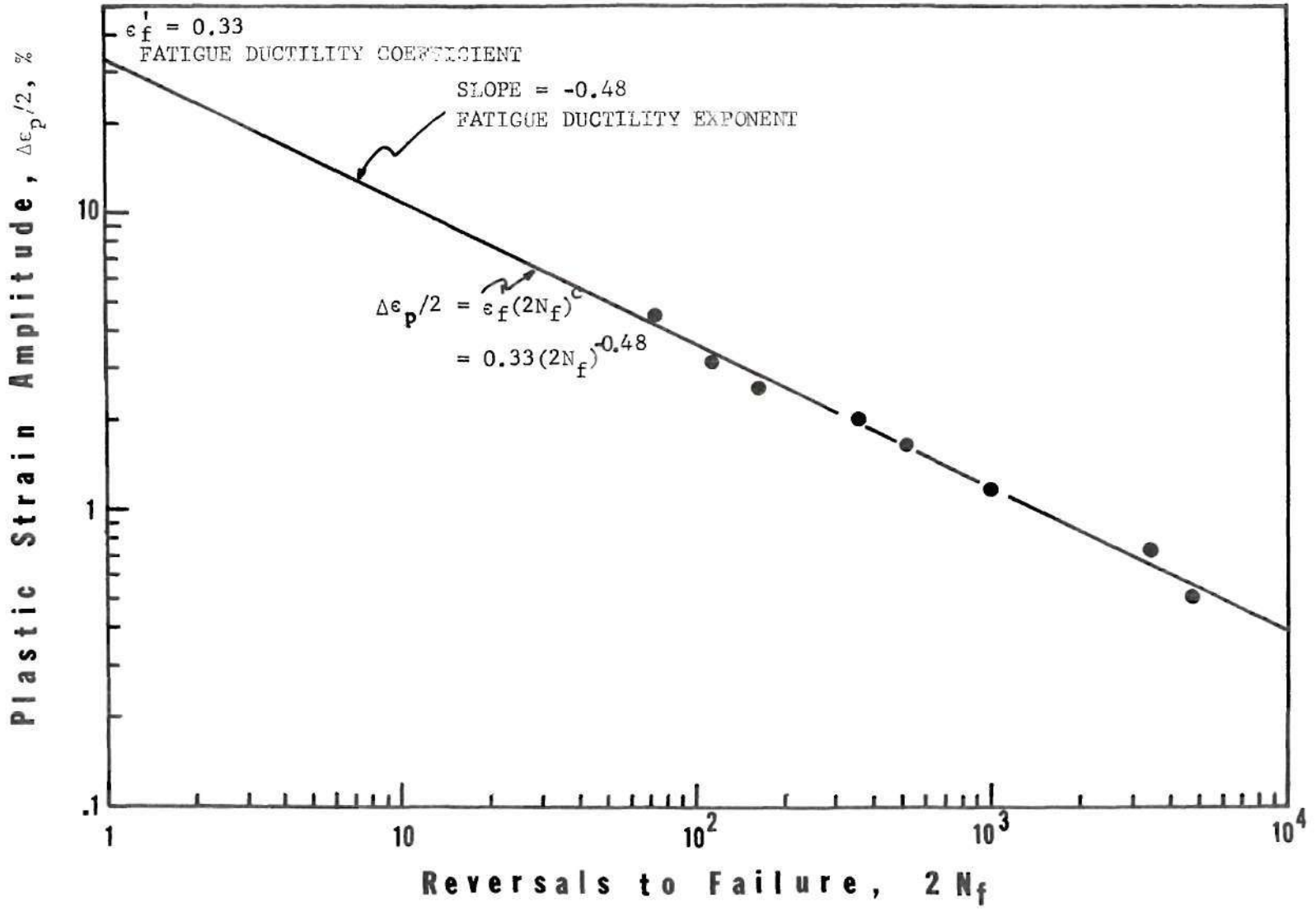


Figure 9. Low Cycle Fatigue Data for Fully Ordered Crystals

straight line can be presented as an equation;

$$\Delta\epsilon_p/2 = \epsilon_f' (2N_f)^c$$

$$= 0.33 (2N_f)^{-0.48}$$

This is the Manson-Coffin low cycle fatigue law for fully ordered $Cu_3Au$ crystals.

Figure 10 shows the low cycle fatigue properties for disordered crystals. The fatigue ductility exponent was found to be c = - 0.6. The fatigue ductility coefficient was $\epsilon_f' = 0.65$. Therefore, the Manson-Coffin low cycle fatigue law for disordered $Cu_3Au$ crystals can be written as

$$\Delta\epsilon_p/2 = \epsilon_f' (2N_f)^c$$

$$= 0.65 (2N_f)^{-0.6}$$

The low cycle fatigue resistance of a material depends both on the fatigue ductility exponent c and the fatigue ductility coefficient $\epsilon_f'$. Figure 11 is a comparison for the low cycle fatigue properties for fully ordered and disordered crystals. At very high strain amplitudes, the disordered crystals are superior to the fully ordered crystals by their higher fatigue ductility coefficients, which are related to the higher fracture strain and also higher ductility of the disordered crystals. As the strain amplitude decreases, the fully ordered crystals become increasingly stronger

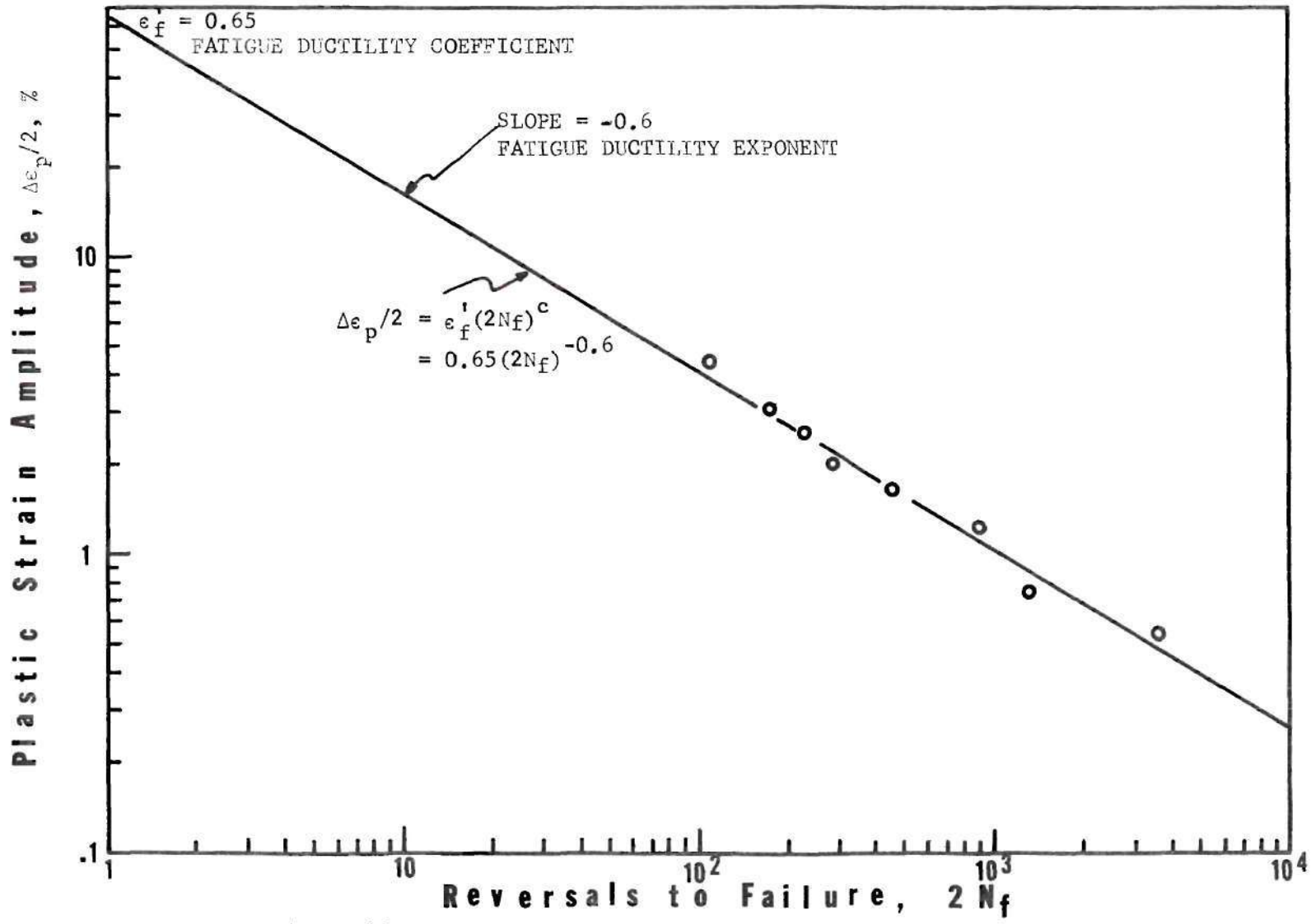


Figure 10. Low Cycle Fatigue Data for Disordered Crystals

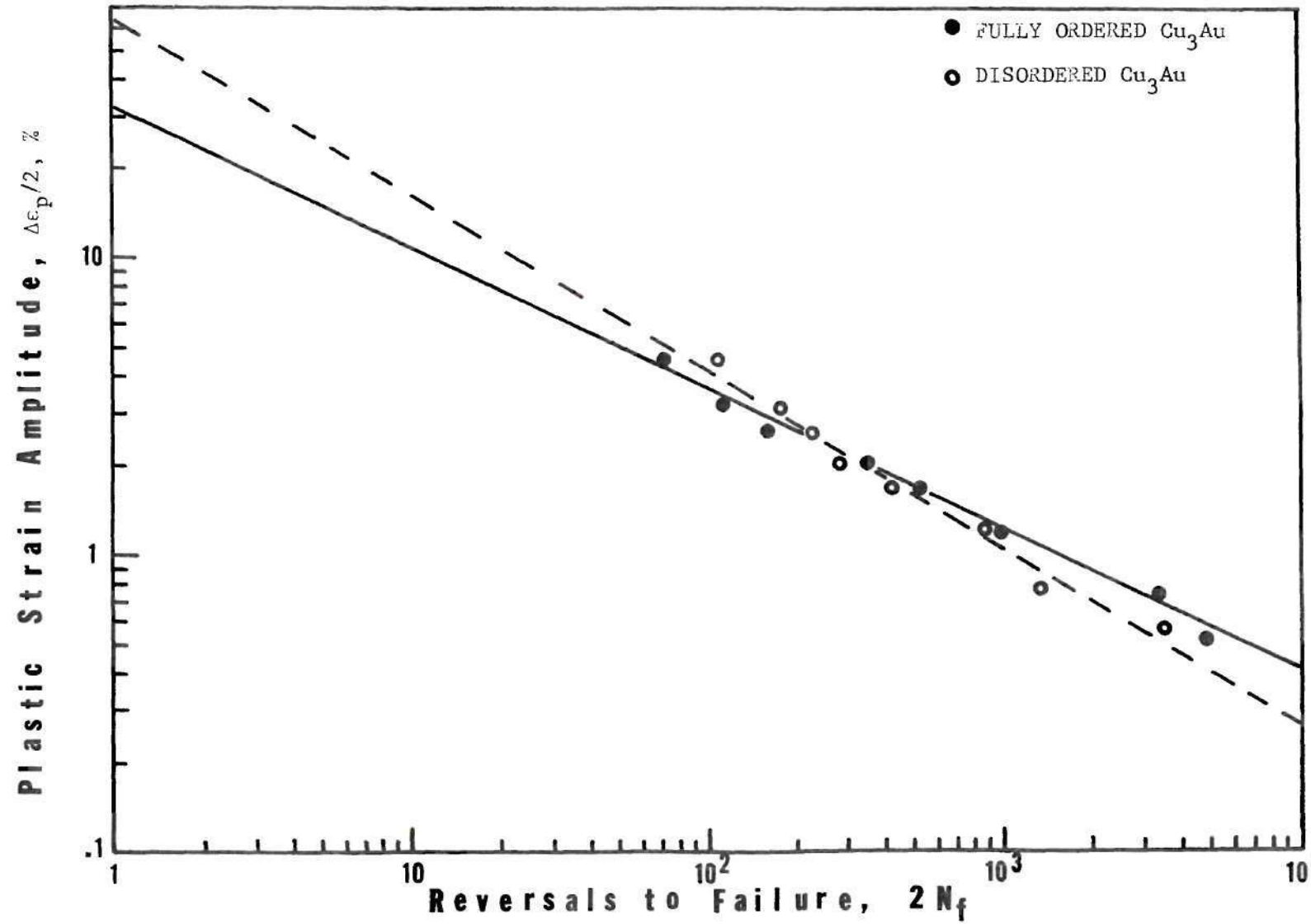


Figure 11. Comparison of the Low Cycle Fatigue Data for Fully Ordered and Disordered Crystals

than the disordered crystals by its higher fatigue ductility exponent. This fact is evidenced in Tables 1 and 2. For instance, at a total shear strain amplitude of ± 10.92%, the disordered crystal has a fatigue life of $N_f$ = 56 cycles, whereas the fully ordered crystal has a fatigue life of only $N_f$ = 36 cycles. At a total shear strain amplitude of ± 1.65%, the disordered crystal has a fatigue life of $N_f$ = 1800 cycles, while the fully ordered crystal has a fatigue life of $N_f$ = 2400 cycles. In Figure 11, it is further noted that the lines cross at a common point at about $2N_f$ = 300 cycles and plastic strain amplitude $\Delta\epsilon_p/2 \approx 2.15\%$. Around this region, the low cycle fatigue resistance of fully ordered and disordered crystals is almost the same.

Another interesting parameter is the ratio $N_o/N_f$, which represents the fraction of total fatigue life involved in nucleating a fatigue crack. Figure 12 is a comparison of the fraction of fatigue life for crack nucleation as a function of plastic shear strain amplitude for fully ordered and disordered crystals. It is apparent that $N_o/N_f$ becomes less as the plastic shear strain amplitude is increased. For the fully ordered crystals, the ratio ranges from 0.4 to 0.6, whereas for the disordered crystals it ranges from 0.6 to 0.8. Therefore, it is clear that the fraction of total fatigue life involved in nucleating a fatigue crack is larger for the disordered crystals than for the fully ordered crystals. Since total fatigue life is the sum of the life involved in nucleating a fatigue crack plus the life involved for the crack to propagate until final failure, we can also claim that the fraction of total fatigue life involved in propagation of a crack until final failure is greater for the fully ordered

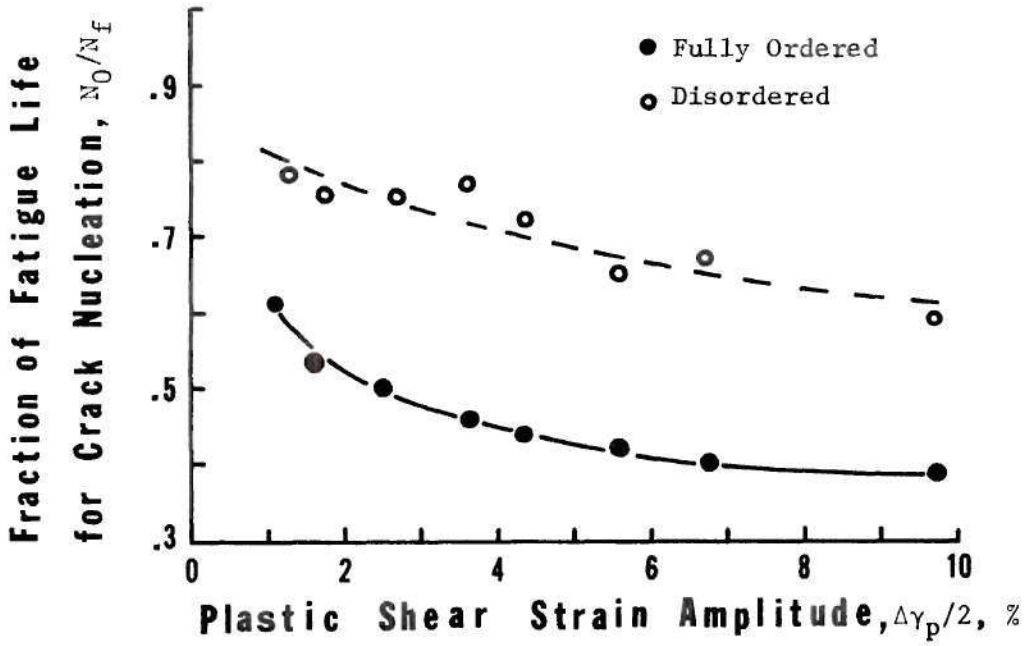


Figure 12. Comparison of the Fraction of Fatigue Life for Crack Nucleation as a Function of Plastic Shear Strain Amplitude for Fully Ordered and Disordered Crystals

crystals than for the disordered crystals. This fact can also be seen in Figures 5 and 6, where an arrow was indicated on each curve at the point where the fatigue cracks were first observed. The final stage of fatigue life, as shown by the rapid softening of the curves due to fatigue crack propagation, is always greater for the fully ordered crystals than for the disordered crystals at the same strain amplitude level.

## 4.4 Cyclic Stress-Strain Curve

The most convenient way to describe cyclic deformation resistance of a metal is the cyclic stress-strain curve. There are a number of methods that can be used for the determination of the cyclic stress-strain curve.[24,25] In the present investigation, since a steady state or saturation condition was never obtained, the half-life data were used to construct the cyclic stress-strain curve for fully ordered and disordered crystals. Figure 13 is the cyclic stress-strain curves for fully ordered and disordered crystals determined from half-life data. The initial part of the monotonic stress-strain curves are included for comparison. It is clear that since both cyclic stress-strain curves are above the monotonic stress-strain curves, we can conclude that both ordered and disordered crystals harden cyclically. But the degree of hardening is not the same. In the monotonic stress-strain curves, the disordered crystal is above the fully ordered crystals, while in the cyclic stress-strain curves the fully ordered crystals are above the disordered crystals. This shows that the fully ordered crystals cyclically harden much more than the disordered crystals. This is related to the much higher strain hardening rate of the fully ordered crystals in tensile test.

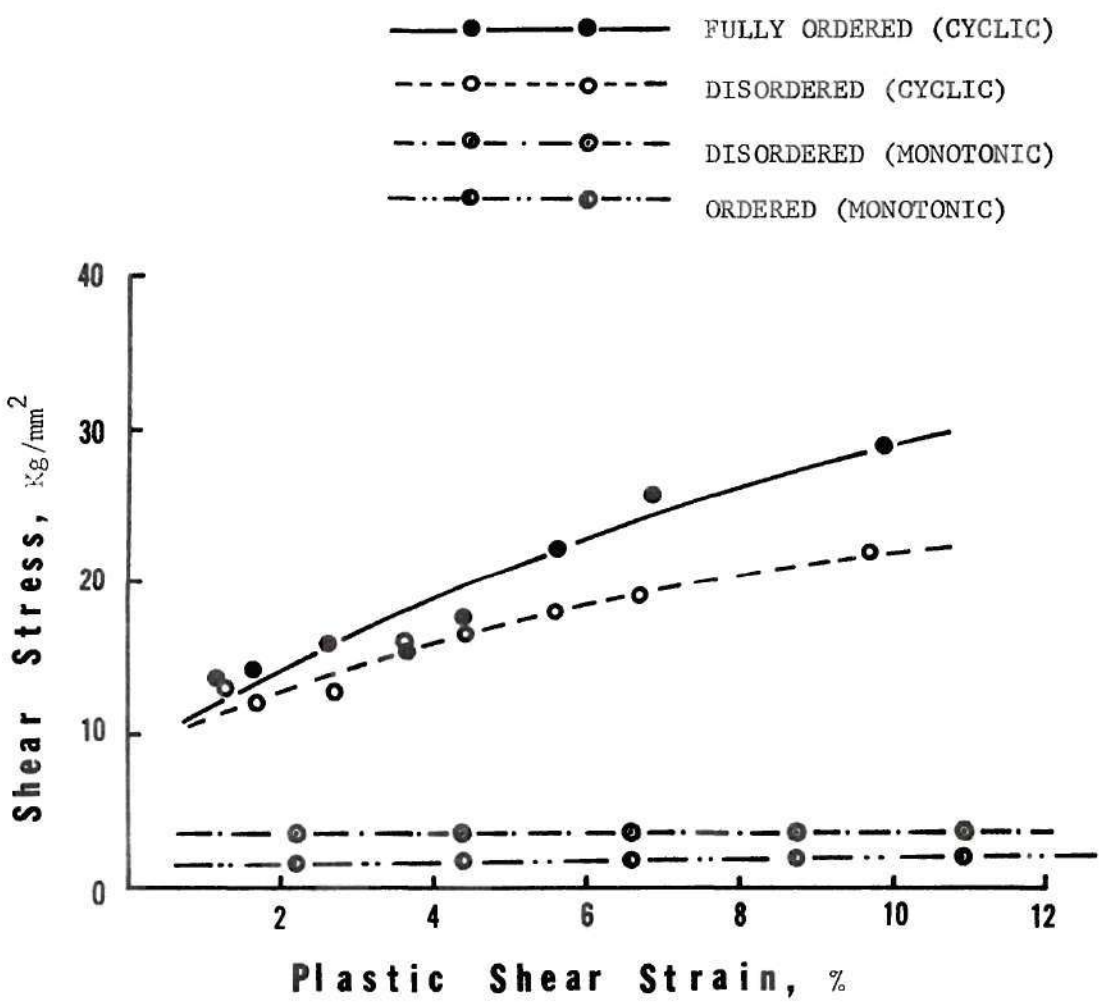


Figure 13. Cyclic Shear Stress-Shear Strain Curves for Fully Ordered and Disordered Crystals. (The Monotonic Shear Stress-Shear Strain Curves Are Also Included for Comparison)

## 4.5 Surface Damage and Fractographic Observations

Since all the low cycle fatigue specimens were electropolished before the tests, the slip lines development and surface damage can be easily observed. Figure 14 is a typical example and shows the initial slip bands of a disordered crystal cyclically strained at a total shear strain amplitude of ± 1.1% for 5 cycles. Slip trace analysis indicated that both fully ordered and disordered crystals deformed by slip on the primary slip system (111) $[\bar{1}01]$ in the early stage of the fatigue life. As the number of cycles increased, however, a deformation band was gradually developed. The formation of the deformation band was believed to be related to the inhomogeneous deformation and lattice reorientation.[26] The pole of the deformation band traces, as determined by trace analysis, almost coincided with the active slip direction $[\bar{1}01]$. The number of cycles spent for the formation of a deformation band increased with decreasing strain amplitude. For instance, at a total shear strain amplitude of ± 10.92%, the deformation band was developed within less than 10 cycles, whereas at a total shear strain amplitude of ± 1.65%, it took hundreds of cycles to develop.

Fatigue cracks were initiated after the deformation bands were developed. The number of cycles, $N_0$, needed to reach this stage depends on both the strain amplitude and the state of order, as can be seen from Tables 1 and 2. In most cases, for both fully ordered and disordered crystals, fatigue cracks were nucleated at the intersection of slip bands and the deformation bands near the grips. Under optical examination, it appeared that the cracks jumped from one slip band to another until finally a macroscopic crack was developed, which then propagated along the

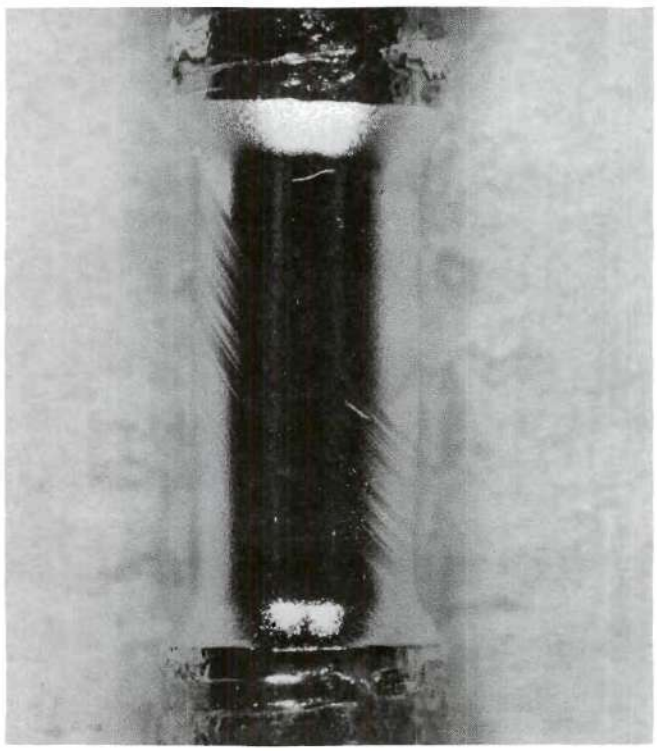

Figure 14. Initial Slip Bands of a Disordered Crystal (Cyclically Strained at $\Delta\gamma_t/2 = \pm 1.1\%$, N = 5 Cycles, Magnification 10X)

boundaries of the deformation bands. Figure 15 is a typical example showing a deformation band and crack nuclei for a fully ordered specimen. In some cases, e.g., lower strain amplitude tests, the deformation band crack propagated across the entire fatigue specimen as shown in Figures 16 and 17. In most cases, cracking occurred on other systems prior to fracture, leading to the so called "cup-cone fracture." Fully ordered crystals had a stronger tendency for this type of fracture than disordered ones because of their higher fracture stress. Stage II type fatigue crack propagation, which is perpendicular to the stress axis, was not observed. Figures 17 and 18 show the appearance of some of the low cycle fatigue specimens of disordered and fully ordered crystals following various strain amplitude tests.

Scanning electron fractographs revealed that the room temperature low cycle fatigue failures were essentially ductile both for fully ordered and disordered crystals as evidenced by the predominance of ductile fatigue striations at low magnification and "shear type fracture" at high magnification, Figures 19 and 20. The most important feature of the fractographic observations, however, is that the stage II fatigue striations have been observed on slant fracture surfaces both for fully ordered and disordered crystals, Figure 21. The result is rather unusual, since some workers believe that it is impossible to produce fatigue striations on slant fracture surfaces.[27]

## 4.6 Transmission Electron Microscopy

Characterization of the fatigue specimens was also performed by use of transmission electron microscopy. Figure 22 shows a typical micrograph

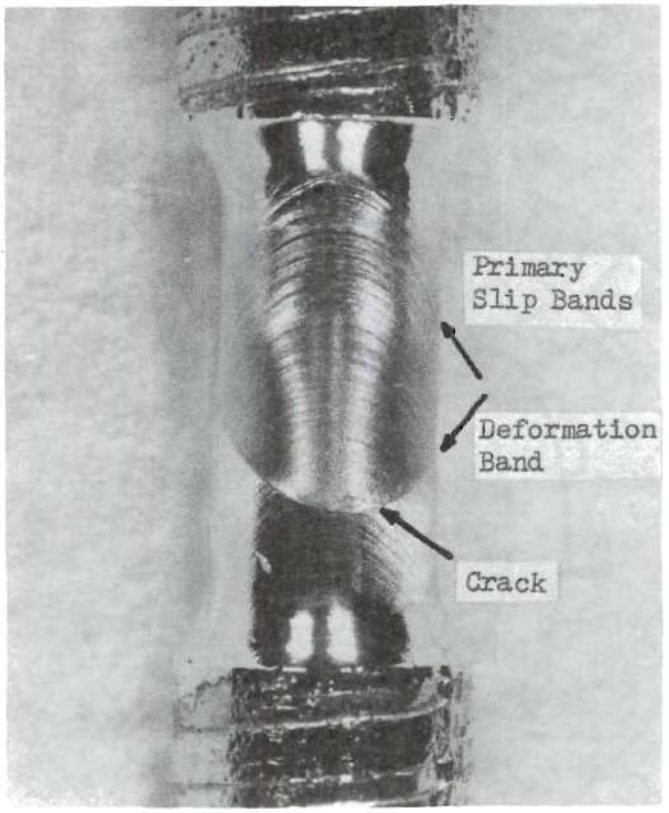


Figure 15. Formation of Deformation Band, and Crack Nucleation at the Intersection of Slip Bands and Deformation Band for a Fully Ordered Specimen. ($\Delta\gamma_t/2 = \pm 4.4\%$, N = 106 Cycles, Magnification 10X)

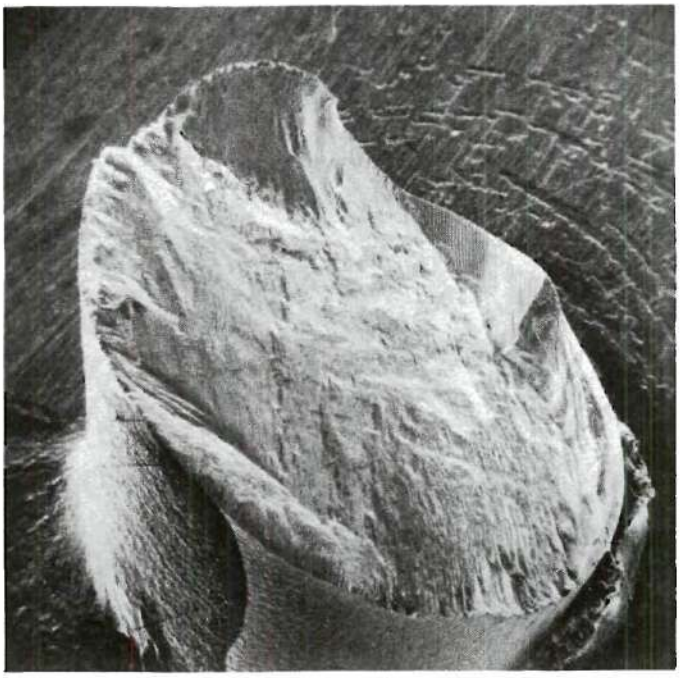

Figure 16. Low Magnification Scanning Electron Fractograph of Fully Ordered Specimen Showing Stage I Fracture Surface. ($\Delta\gamma_t/2 = \pm 1.65\%$, $N_f = 2400$ Cycles, Magnification 25X)

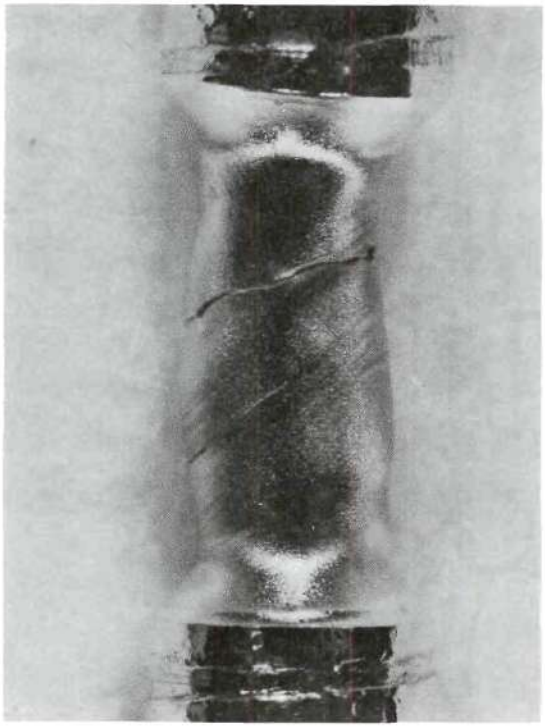

(a)

(b)

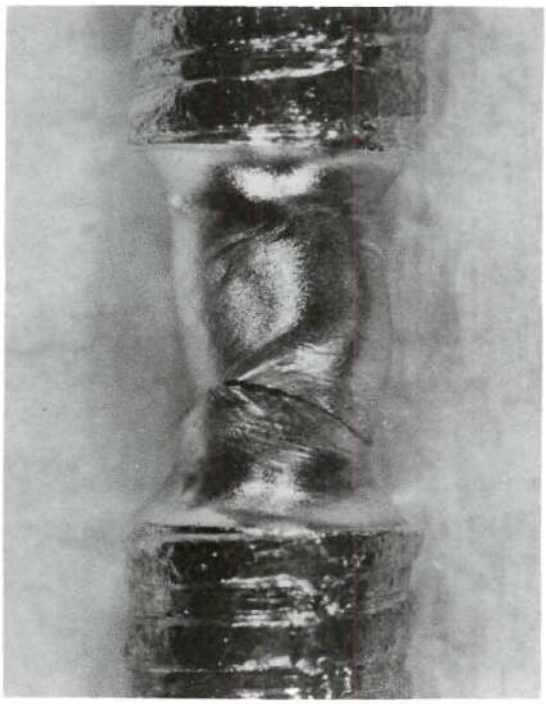

(c)

Figure 17. Appearance of Specimens of Disordered Crystals Following Low Cycle Fatigue Tests: ((a) $\Delta\gamma_t/2 = \pm 1.65\%$, $N_f = 1800$ Cycles (b) $\Delta\gamma_t/2 = \pm 5.23\%$, $N_f = 144$ Cycles (c) $\Delta\gamma_t/2 = \pm 7.80\%$, $N_f = 89$ Cycles, Magnification 10X)

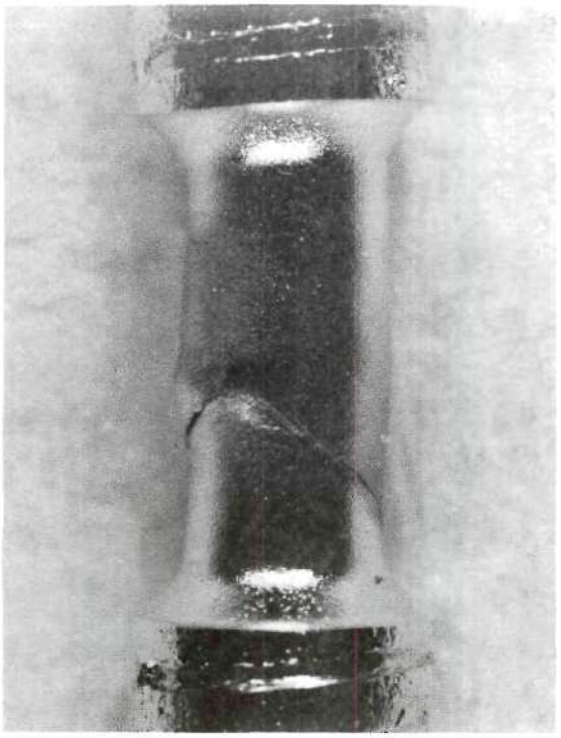

(a)

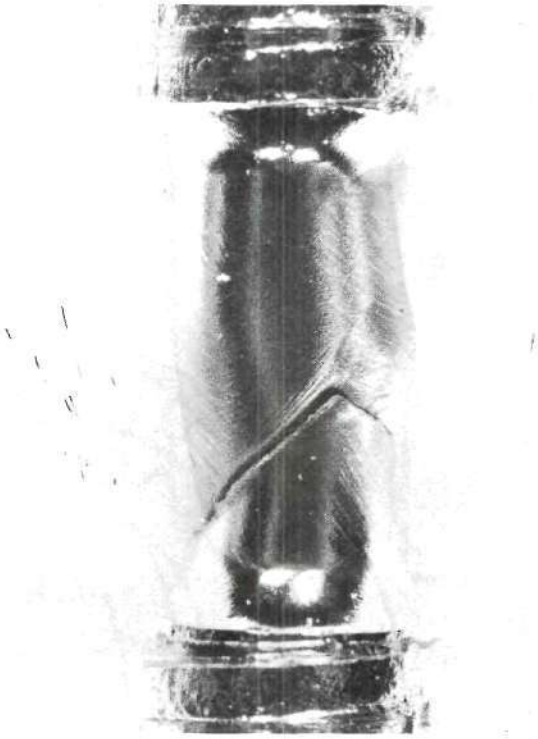

(b)

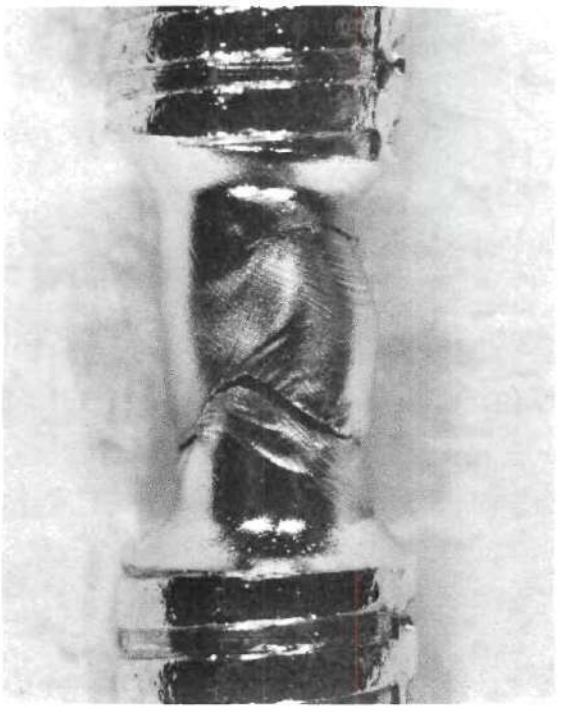

(c)

Figure 18. Appearance of Specimens of Fully Ordered Crystals Following Low Cycle Fatigue Tests: ((a) $\Delta\gamma_t/2 = \pm 1.65\%$, $N_f = 2400$ Cycles (b) $\Delta\gamma_t/2 = \pm 3.30\%$, $N_f = 496$ Cycles (c) $\Delta\gamma_t/2 = \pm 6.58\%$, $N_f = 81$ Cycles, Magnification 10X)

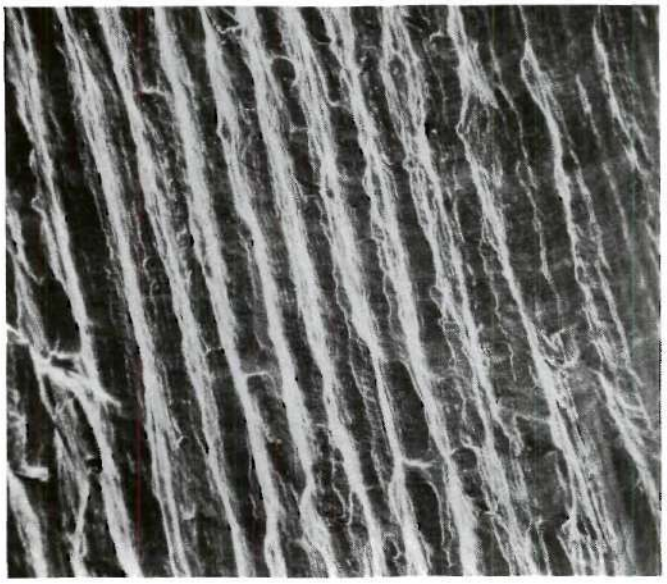

(a)

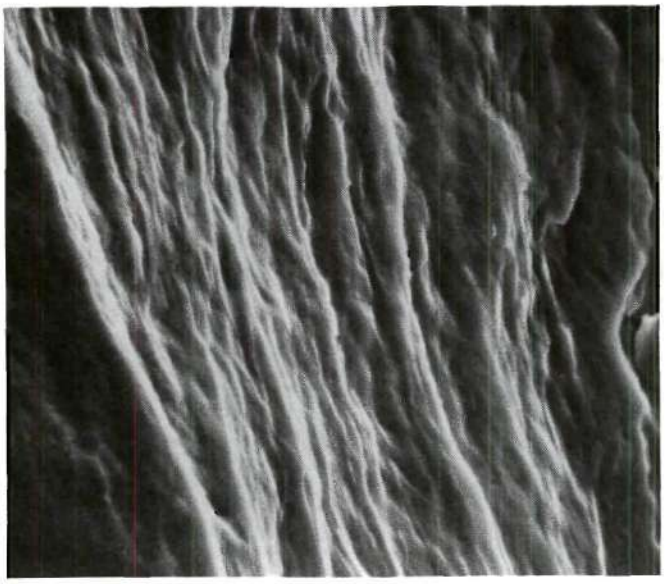

(b)

Figure 19. Scanning Electron Fractographs of Fully Ordered Specimen. ($\Delta\gamma_t/2 = \pm 5.23\%$, $N_f = 180$ Cycles, (a) Magnification 240X, Showing Fatigue Striations, (b) Magnification 6200X, Showing "Shear Fracture" Features)

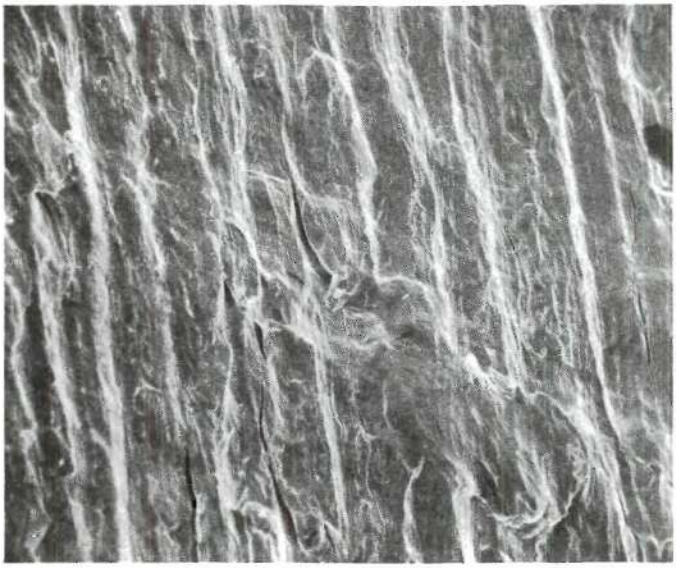

(a)

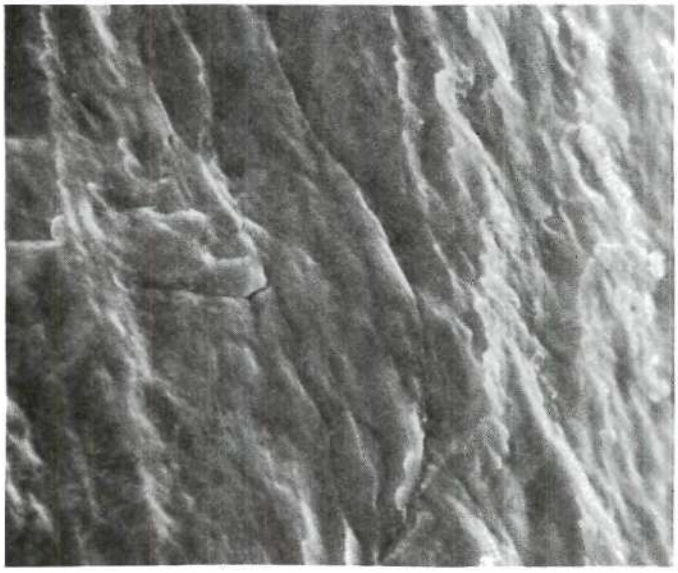

(b)

Figure 20. Scanning Electron Fractographs of Disordered Specimen. ($\Delta\gamma_t/2 = \pm 5.23\%$, $N_f = 144$ Cycles, (a) Magnification 220X, Showing Fatigue Striations, (b) Magnification 6000X, Showing "Shear Fracture" Features)

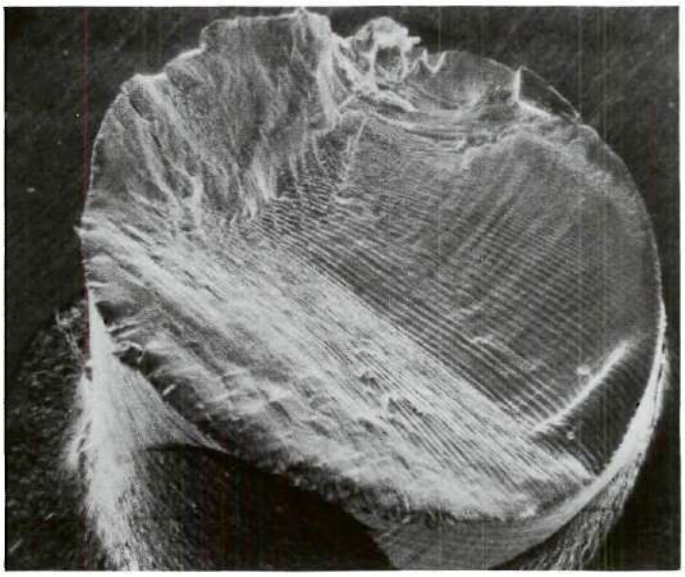

(a)

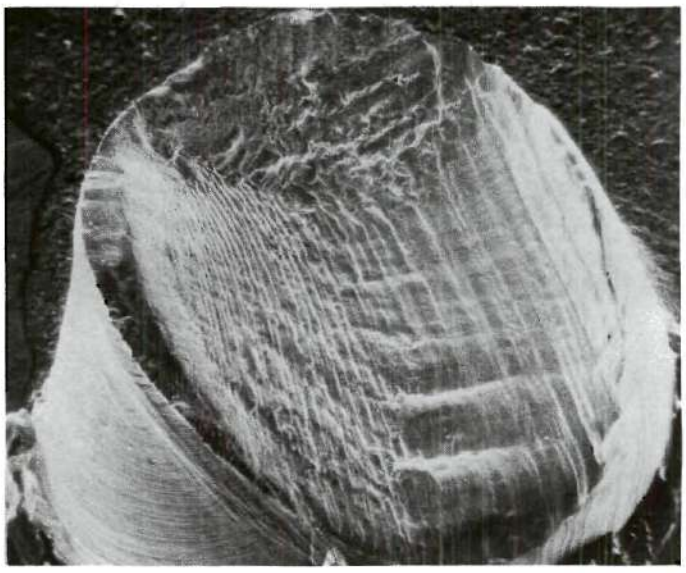

(b)

Figure 21. Scanning Electron Fractographs Showing Stage II Fatigue Striations on Slanted Fracture Surfaces. ((a) Fully Ordered, $\Delta\gamma_t/2 = \pm 5.23\%$, $N_f$ = 180 Cycles, Magnification 25X, (b) Disordered, $\Delta\gamma_t/2 = \pm 5.23\%$, $N_f$ = 144 Cycles, Magnification 27X)

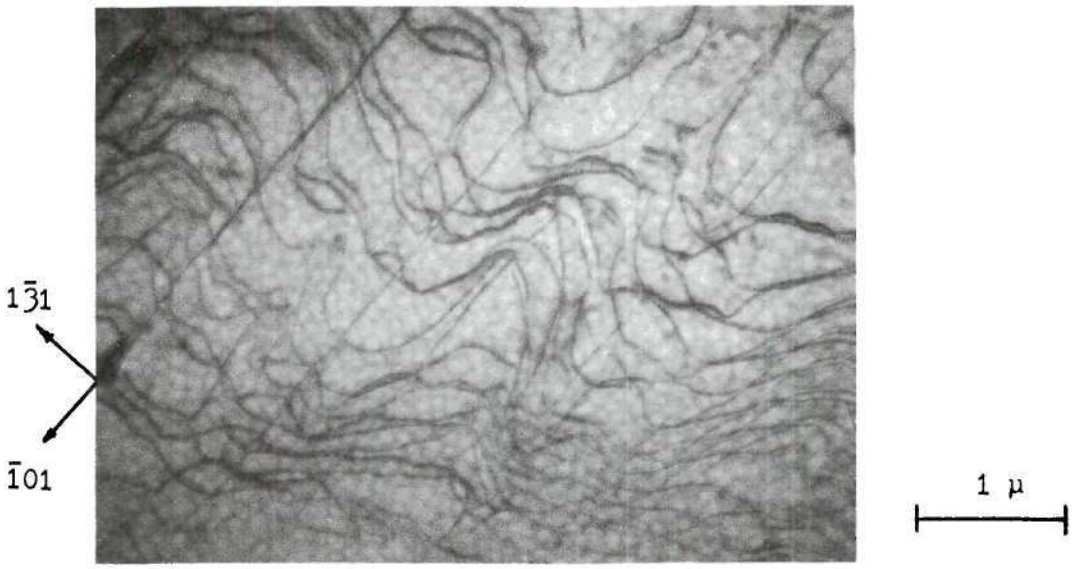


Figure 22. Transmission Electron Micrograph Showing Dislocation Arrangements in a Fatigued Disordered Crystal. ($\Delta\gamma_t/2 = \pm$ 1.1%, N = 30 Cycles. The plane of the micrograph is approximately (323) or 10.02 deg from the primary (111) slip plane)


Figure 23. Transmission Electron Micrograph Showing Dislocation Arrangements in a Fatigued Fully Ordered Crystal. ($\Delta\gamma_t/2 = \pm$ 1.1%, N = 30 Cycles. The plane of the micrograph is (221) or 15.79 deg from the primary (111) slip plane)

of a disordered specimen cyclically strained at a total shear strain amplitude of ± 1.1% for 30 cycles. The dislocations are in fairly uniformly spaced groups in the primary slip planes and in various orientations. The majority of dislocations are primary (111) $[\bar{1}01]$ edge dislocations on parallel slip planes.

The most important features of the dislocation microstructure in the disordered crystals subjected to fatigue deformation is the formation of dislocation dipoles. It has been proposed that the dipoles form by the dragging of jogs in screw dislocation[28] as well as by the mutual interaction and alignment of parallel edge dislocations of opposite sign.[29] The result is consistent with that reported by previous workers.[30] When tension-compression loads are applied, dislocation dipoles and cells are the most commonly observed structures in fatigued f.c.c. metals. A dislocation cell structure was not observed in the disordered $Cu_3Au$ crystals.

A typical micrograph of the dislocation configuration in a fully ordered specimen, which was cyclically strained at a total shear strain amplitude of ± 1.1% for 30 cycles, is shown in Figure 23. In most cases the dislocations are uniformly distributed and the majority of the dislocation segments are in screw orientations, i.e., parallel to the primary slip direction $[\bar{1}01]$. It is difficult to know from the particular orientation shown in Figure 23 whether the pairs are lying in the primary slip plane or in some cross-slip plane. However in those cases where the points of emergence of the dislocation pairs with the foil surface can be clearly observed, they appear to lie on a (010) slip trace, i.e., the cross-slip plane first reported by Kear,[12,31] by Mikkola and Cohen,[19] and also by Czernichow and Marcinkowski.[16] Cross slip of the screw segments onto

(010), with the mixed edge and screw segments remaining in (111), is a favorable process since the energy of the superlattice dislocation is reduced.[13] This is because the nearest neighbor energy of the connecting strip of antiphase boundary of the superlattice dislocation vanishes in the cube plane with a consequent lowering of the total energy of the superlattice dislocation.

The fatigue-induced dislocation structures for both fully ordered and disordered crystals developed at the early stage of the fatigue hardening curves strikingly resemble those found in unidirectional hardening reported by previous workers.[12,16,19,31] As mentioned earlier, cross-slip of the superlattice dislocations onto (100) type plane is believed responsible for the high rate of strain hardening in ordered crystals. From the present result, it is apparent that this same hardening mechanism is also responsible for the fatigue hardening of fully ordered crystals. This is in agreement with the suggestion by Feltner and Laird[30] that a strong parallel in deformation processes exists between cyclically and unidirectionally hardening in single phase materials.

Figure 24 shows the antiphase domain boundary structure in a fully ordered crystal cyclically strained at a total shear strain amplitude of ± 1.1% for 30 cycles. The two most important features of the APB's in Figure 24 are (1) that the original grown-in cube orientation domain structure has been distorted by the slip process and (2) that the APB's show a strong tendency to lie on cube planes. This can be seen by comparing the traces of the cube planes shown in the figure.

Antiphase domain boundaries were found also associated with dislocation structures in the thicker regions of the foil. Figure 25 is a

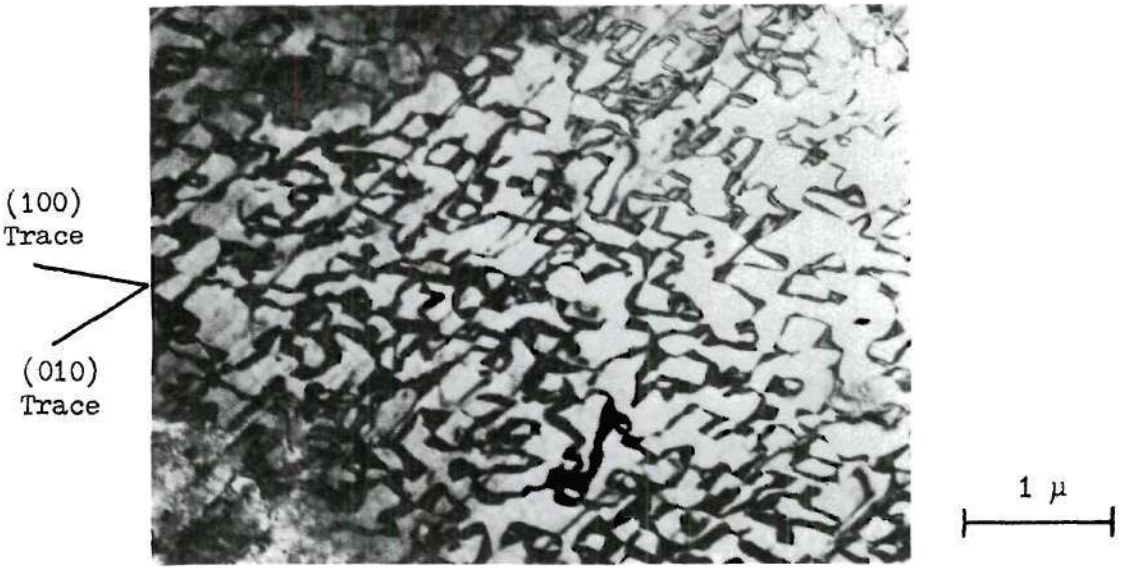


Figure 24. Bright Field Transmission Electron Micrograph of Antiphase Boundaries in a Fatigued Fully Ordered Crystal. ($\Delta\gamma_t/2 = \pm 1.1\%$, N = 30 Cycles. The plane of the micrograph is (221).)

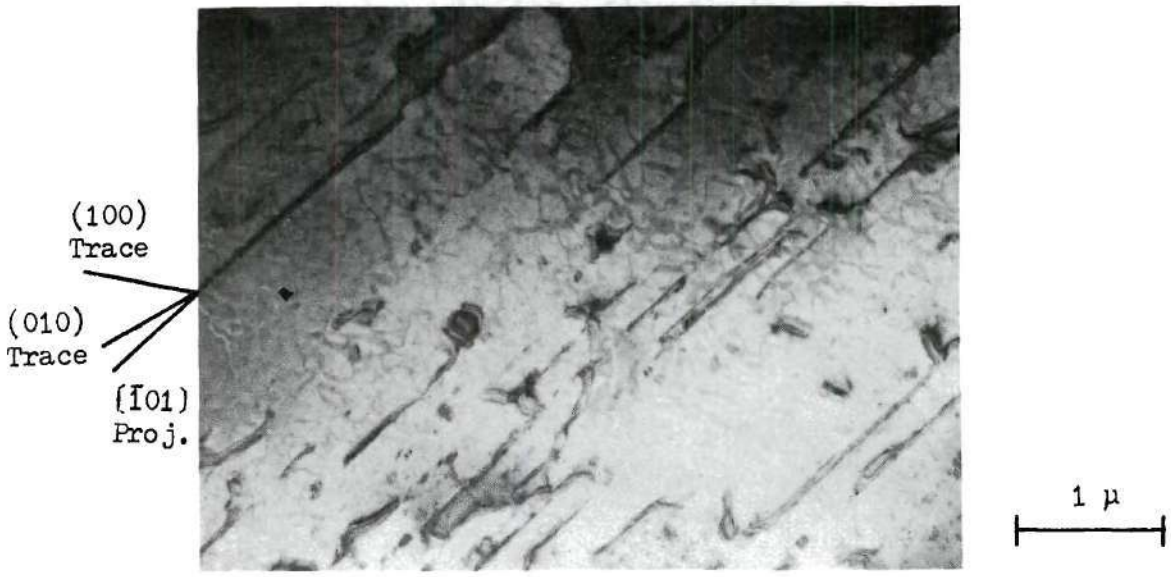


Figure 25. Antiphase Boundaries and Dislocations in the Same Area of a Thin Foil of a Fatigued Fully Ordered Crystal. ($\Delta\gamma_t/2 = \pm 1.1\%$, N = 30 Cycles. The plane of the micrograph is (221).)

transmission electron micrograph which shows both the APB's and dislocations in the same area of a foil in a fully ordered crystal cyclically strained at a total shear strain amplitude of ± 1.1% for 30 cycles. Because of the gradual change in orientation of this foil, the APB's do not appear in the bottom right hand corner of the micrograph, while in the rest of the micrograph they are just visible under the present conditions. Examination of the micrographs in both dislocation and antiphase contrast shows no direct evidence of dislocation/domain boundary interaction.

# CHAPTER V

# DISCUSSION

## 5.1 Fatigue Hardening/Softening

Repeated loading of a metal between fixed limits of strain will produce either hardening or softening, depending on the initial condition of the metal, the strain amplitude, and the test temperature. Fatigue hardening is somewhat more complex than the case of monotonic strain hardening, mainly because of the added complications of strain reversal and strain repetition. Generally speaking for a metal, an annealed material will fatigue harden and a cold-worked material may fatigue soften. The softening rate of the cold worked materials increases as the strain amplitude decreases while the hardening rate of the annealed materials increases with increasing strain amplitude.[32]

Annealed f.c.c. metals generally show two stages of fatigue hardening: an initial stage of rapid hardening followed by a stage of saturation or steady state. For most materials the first stage is usually complete from a few percent to about 50% of the total lifetime. The steady state stress is determined only by the plastic strain amplitude and temperature of testing in materials of wavy slip mode, whereas when the mode of slip is planar the steady state stress is sensitively dependent on the deformation and thermal history.[32] It is further noted that single crystals respond to cycling in a manner similar to that of the fully annealed materials.[33]

Examination of Figures 5 and 6 indicates that the fatigue hardening/softening for the fully ordered and disordered crystals are unusual for an annealed f.c.c. metal. A steady state or saturation condition has never been obtained both for fully ordered and disordered crystals. The complete fatigue hardening/softening for the fully ordered crystals consist of three stages: an initial stage of rapid hardening, followed by a stage of softening, and a final stage of very slow softening. The missing of the final stage at intermediate shear strain amplitude tests, and the missing of the second and final stages at higher shear strain amplitude tests is attributed to the formation and propagation of fatigue cracks.

A quantitative explanation of the fatigue hardening/softening is still very difficult at the present time because many mechanisms can play a role. For instance, for a solid solution alloy, Cottrell[34] has pointed out that the various types of interactions, elastic, electrical, chemical, and geometrical, that occur between solute atoms and dislocations all play a role in undirectional hardening. These problems clearly apply to the cyclic case which appears remarkably similar in mechanism to the undirectional situation but suffers the additional complication of more complex dislocation structures.[30,32] Therefore, only a qualitative treatment of fatigue hardening/softening in this study is appropriate.

In the monotonic strain hardening, for the fully ordered crystals, it is generally believed that cross-slip of the superlattice dislocations to a plane of lowest antiphase boundary energy, which is {100} for ordered $Cu_3Au$,[13] makes further motion of the dislocation difficult. This same hardening mechanism is expected to play an important role in the fatigue

hardening of fully ordered crystals, as evidenced by the transmission electron micrograph, Figure 23.

It is believed that the fatigue softening, which follows the initial hardening for the fully ordered crystals, is due to the disordering of the crystals. Mikkola and Cohen[19] have shown that for $Cu_3Au$ the long-range order parameter S decreased as the plastic strain increased. Researches into the mechanisms of fatigue softening have all shown that softening is the result of degradation of the original hardening microstructure by continuous back and forth motion of dislocations through that microstructure.[35] The ability of the hardening microstructure to resist dislocation motion will determine its stability. Microstructures most susceptible to fatigue softening are generally those strain-hardened and precipitate hardened structures. Calabrese and Laird,[36] after studying the cyclic stress-strain response of solution-treated Al-4% Cu alloy and aged alloy with coherent θ" precipitates, have concluded that previous explanations for cyclic softening and poor fatigue properties such as overaging, reversion, and aging inhomogeneities have been shown to be inappropriate in most alloys. They further pointed out that cyclic softening is due to the disordering of the ordered precipitates, and suggest that if the precipitates are not ordered no softening will be observed. From the present results, it is apparent that the fatigue hardened $Cu_3Au$ ordered structure falls into this same category.

The role of antiphase domain boundaries in the fatigue hardening of fully ordered crystals is not clear. In a review of the properties of ordered alloys,[37] Cohen concluded that the domain boundary itself does not seem to play a direct role in the strain-hardening of ordered alloys.

Marcinkowski[38] also pointed out that since there are no pile-ups of dislocations at the antiphase domain boundaries, there does not seem to be any strong resistance caused by these boundaries. The forces on the dislocations are probably high enough so that they cut through antiphase domain boundaries without any trouble.

The continuous fatigue hardening until fracture for the disordered crystals is also unusual. Since the disordered $Cu_3Au$ single crystals are not truly disordered but contain short-range order,[39] it is reasonable to believe that the continuous hardening of the disordered crystals until fracture may be associated with the presence of short-range order. A review on the effect of short-range order on mechanical properties has been given by Cahn,[40] and Fisher[41] was the first to recognize that short-range order must influence the strength of a solid solution by increasing the frictional drag on a moving dislocation. The reduction in the number of unlike nearest-neighbor bonds consumes energy, which is provided through the increased stress required to move the dislocation. In the fatigue hardening of disordered crystals, the decisive factor in the slip process seems to be the interaction between glide dislocation and short-range order. As a result of dislocation-dislocation, and short-range order-dislocation interactions, the dislocation should have little opportunity to form a cell structure. This is clearly demonstrated in the transmission electron micrograph, Figure 22. Grosskreutz and Hancock,[42] who studied the mechanisms of fatigue hardening in Cu single crystals, have concluded that the "shuttle" of dislocations to and fro within the cell walls is responsible for the "saturation hardening." The inability to develop dislocation cell structures during fatigue could be responsible for the

continuous hardening (without saturation) that is observed for the disordered crystals prior to crack initiation.

## 5.2 Low Cycle Fatigue Resistance

One of the purposes of this study was to determine how well the Manson-Coffin relationship

$$\Delta\epsilon_p/2 = \epsilon_f'(2N_f)^c$$

is obeyed and also to determine the fatigue ductility exponent, c, and the fatigue ductility coefficient, $\epsilon_f'$, both for fully ordered and disordered crystals. The results in Figures 9 and 10 indicate that the Manson-Coffin law is a good approximation of the low cycle fatigue behavior of $Cu_3Au$ single crystals both in fully ordered and disordered state.

Many investigators have attempted to relate plastic strain resistance with monotonic true fracture strain, $\epsilon_f$.[43-45] No general agreement is found between investigators with approximations of $\epsilon_f'$ ranging from 0.35 $\epsilon_f$ to $\epsilon_f$. For fully ordered crystals, $\epsilon_f$ has been calculated as 0.47, and the value of $\epsilon_f'$ obtained from Figure 9 is 0.33. Therefore, the relation

$$\epsilon_f' = 0.70\ \epsilon_f$$

was obtained for fully ordered crystals. For the disordered crystals, the calculated value of $\epsilon_f$ is 0.69, and the value of $\epsilon_f'$ obtained from Figure 10 is 0.65. Therefore the relation

$$\epsilon_f' = 0.94\ \epsilon_f$$

was obtained for disordered crystals. The lower value of the ratio $\epsilon_f'/\epsilon_f$ for fully ordered crystals, 0.70, as compared to the value for disordered crystals, 0.94, could be related to the breakdown of the initial hardening microstructure and subsequent fatigue softening for the fully ordered crystals.

The value of c is reported to range from -0.5 to -0.7.[24] Experimentally, c is observed to vary with material and testing conditions. In the present investigation, the values of c obtained from Figures 9 and 10 were -0.48 and -0.6 for fully ordered and disordered crystals, respectively. These values lie within the range of values reported for most metals.

Since both the fatigue ductility coefficient, $\epsilon_f'$, and the fatigue ductility exponent, c, contribute to the low cycle fatigue resistance, both of these effects need be considered in comparing the low cycle fatigue resistance of various materials. As mentioned earlier, and shown in Figure 11, at very high strain amplitudes the disordered crystals are superior over the fully ordered crystals by their higher fatigue ductility coefficient. As the strain amplitude decreases, the fully ordered crystals become increasingly stronger than the disordered crystals by their higher fatigue ductility exponent. This point will be discussed in more detail in the following paragraphs.

It is generally believed that since ordering strongly inhibits connecting cross-slip*, it will retard crack nucleation. In the same way,

---

*Connecting cross-slip, in which screw dislocations cross-slip far enough to bypass barriers on their slip planes and propagate on neighboring slip planes, thus leads to the formation of coarse slip bands, Ref. 46.

it will increase resistance to crack propagation by increasing the plastic work at the crack tip.[46,47] Therefore, the ordered crystals are expected to have superior fatigue resistance both in crack nucleation and crack propagation when compared to the disordered crystals. This analysis has been used to explain the improvements in fatigue strength under stress cycling conditions for $Ni_3Mn$ and Fe-Co-V.[2]

For strain-controlled low cycle fatigue, the situation is quite different. The plastic strain is usually large enough to break down the long-range ordered structure. This is evidenced in the fatigue softening of the fully ordered crystals after an initial hardening. Feltner and Beardmore[48] have claimed that the breakdown of the long-range ordered structure does not decrease the fatigue life because ordering results in a more planar slip character and a resultant homogenization of slip which apparently outweighs any effects of strain concentration due to local softening. This is only true for the lower plastic strain range. As the plastic strain amplitude increases, the strain concentration due to local softening will cause the fatigue crack to nucleate prematurely. With further increases, the premature fatigue crack nucleation will outweigh any advantages of the ordered crystals due to stronger resistance to crack propagation. This results in the shorter fatigue life for the fully ordered crystals than for the disordered crystals at very high plastic strain amplitudes as clearly shown in Tables 1 and 2.

## 5.3 Cyclic Stress-Strain Curve

The cyclic stress-strain curves for fully ordered and disordered crystals shown in Figure 13 can also be represented as the log-log plot

of the shear stress amplitude, $\Delta\tau/2$, versus plastic shear strain amplitude, $\Delta\gamma_p/2$, taken from half-life data. Figure 26 is such a curve for fully ordered crystals. The data can be correlated with the equation

$$\Delta\tau/2 = 60(\Delta\gamma_p/2)^{0.36}$$

The value 0.36 is the cyclic strain hardening exponent, n', for fully ordered crystals, which is a little higher than expected, since it has been reported that values of n' fall in the range of 0.1 to 0.25 for most materials.[35]

Figure 27 is the cyclic stress-strain curve for disordered crystals represented as log $\Delta\tau/2$ versus log $\Delta\gamma_p/2$. The data can be presented by the equation

$$\Delta\tau/2 = 41(\Delta\gamma_p/2)^{0.28}$$

where n' = 0.28 is the cyclic strain hardening exponent for disordered crystals, which is close to the range of values reported for most materials.

For comparison, the monotonic strain hardening exponent, n, for fully ordered and disordered crystals is also included in Figures 26 and 27, respectively, where n = 0.13 for fully ordered and n = 0.03 for disordered crystals. Landgraf[25] discusses the empirical correlation between n and cyclic stability. Metals with high n can be expected to cyclically harden, while those with low n can be expected to soften. Materials with $0.1 < n < 0.2$ are stable under fatigue loading. It is apparent that this does not correlate well with the present investigation.

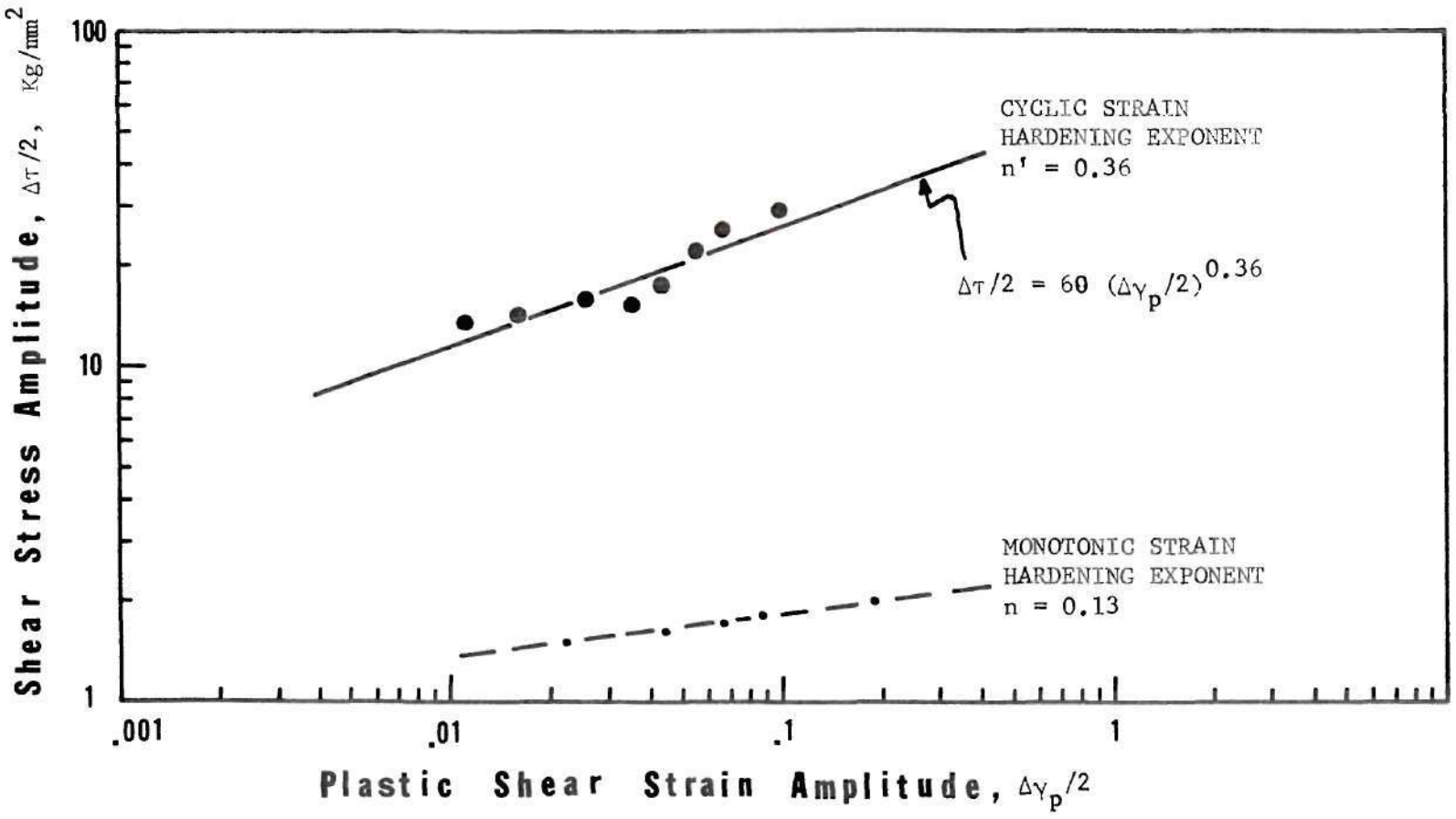


Figure 26. Cyclic Stress-Strain Curve for Fully Ordered Crystals (Represented as log $\Delta\tau/2$ vs log $\Delta\gamma_p/2$. The monotonic strain hardening exponent is also included for comparison.)

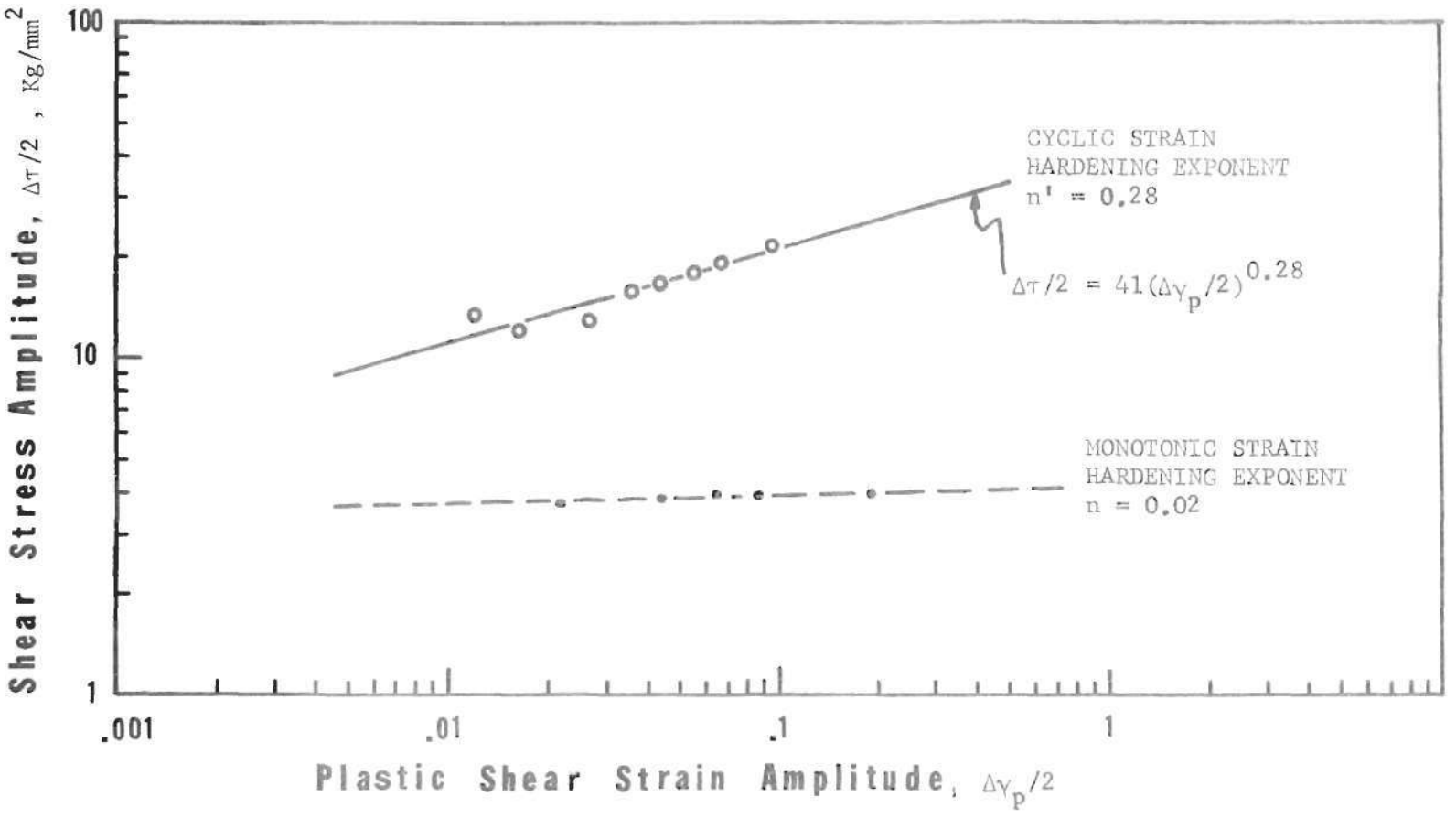


Figure 27. Cyclic Stress-Strain Curve for Disordered Crystals (Represented as log $\Delta\tau/2$ vs log $\Delta\gamma_p/2$. The monotonic strain-hardening exponent is also included for comparison.)

Semiempirical relation between c and n' has been given by Morrow,[24]

$$c \cong - 1/(1 + 5n')$$

For fully ordered crystals, we have

$$c = - 0.48 \qquad n' = 0.36$$

for disordered crystals

$$c = - 0.6 \qquad n' = 0.28$$

As can be seen, the result does not fit the above equation very well. For single crystals of $Cu_3Au$

$$c \cong - 1/(1 + 3n')$$

for both fully ordered and disordered crystals.

## 5.4 Deformation Band (or Kink Band)

Another interesting observation in this study is the formation of deformation bands. As mentioned earlier, the formation of the deformation bands is believed to be related to the inhomogeneous deformation and lattice reorientation.[26] In the extension of aluminum single crystals, Collins and Mathewson[49] first noted a banded appearance and the intimate connection of this banded appearance with the recrystallization behavior. The crystallography of the band is now well established for f.c.c. metals in that

in the early stages of deformation, they form on planes normal to the active slip direction, which is <110>.[50] The mechanism for their formation has been explained by flexual gliding, i.e., an inhomogeneous rotation about an axis in the slip plane and roughly $90^{o}$ to the slip direction. The formation of deformation bands has been found to be orientation-dependent. In the case of aluminum during tension, crystals oriented near <111> do not lead to band formation.[50]

In cyclic deformation, the formation of deformation bands has also been observed. In the study of fatigue hardening in niobium single crystals, Doner et al.[51] observed that, in crystals oriented for single slip, deformation bands developed on their side faces during the rapid hardening stage. They further noted that no deformation bands were observed in crystals which deformed by slip in more than one system. They believed that the presence of macroscopic secondary slip interferes with the formation of the deformation bands. In a study of bending fatigue of aluminum bicrystals, Chin and Backofen[52] observed that deformation bands were found at high and intermediate deflections (lives of about 35,000 and 100,000 cycles, respectively). The deformation bands became the sites of intense substructure formation at the later stages of the fatigue process, with subsequent cracking along the substructure boundaries.

In the present study, the deformation bands were produced in both fully ordered and disordered specimens for all strain amplitudes investigated. The pole of the deformation bands coincided with the primary slip direction $[\bar{1}01]$; consistent with previous work. It is particularly interesting that deformation-band cracking became the predominant factor in the

fracturing process both for the fully ordered and disordered crystals. This will be discussed in more detail in the following section.

## 5.5 Fracture

It is useful to present initially the concept of fracture under cyclic straining in f.c.c. materials in order that it can be used as a model for comparison with fracture in the $Cu_3Au$ alloy used in this study. The process of fatigue in f.c.c. structures may be considered to consist of three stages: fatigue crack nucleation followed by two separate stages (I and II) of crack propagation.[53,54] Generally, fatigue cracks initiate in slip bands or a localized region because of the concentration of plastic strain. The criterion for slip bands cracking is the range of resolved shear stress on the slip plane. Consequently, cracks will initiate on those planes most closely aligned with the maximum resolved shear stress. Stage I crack propagation, which is governed by the local shear stress, is the growth of the crack along well defined slip bands, or coherent twin boundaries, or deformation band boundaries, as in the case of the present investigation, with the crack having an angle of approximately $45^{o}$ to the stress axis. Stage I fatigue fracture surfaces are normally featureless since it involves slip on crystallographic planes. The stage I crack growth eventually changes to stage II type propagation perpendicular to the stress axis. Stage II crack growth depends on the value of the maximum principal tensile stress operating in the region of the crack tip. Stage II crack propagation is generally characterized by well defined striations on the fracture surface. The proportion of the fatigue life spent in each of these stages depends on both the material characteristics and the testing conditions.

In the present study, both the fully ordered and disordered crystals are rather unusual in that they exhibit extensive stage I fractures--deformation band cracking. Fatigue cracks were observed to nucleate at the intersection of slip bands and deformation bands near the grips, as shown in Figure 15. With continued cycling these cracks progressed by jumping from one slip band to another until finally a macroscopic crack developed, which then propagated along the deformation-band boundaries. In some cases, this deformation band cracking progressed across the entire fatigue specimen, whereas in most cases cracking occurred on other systems prior to fracture, leading to the so called "cup-cone fracture." Stage II type fatigue crack propagation was never observed.

While it is generally held that fatigue fractures are transcrystalline fractures, deviation from this tendency is not unusual. For instance, coherent twin boundaries frequently act as preferred sites for both persistent slip bands and early fatigue cracks.[55] Several workers have suggested a number of reasons, but did not reach any firm conclusion. The reason for the extensive deformation band cracking observed both in fully ordered and disordered $Cu_3Au$ is not well understood. It is believed that the extrusion-intrusion process is exaggerated at the interaction of slip band and deformation band boundaries as suggested by Hull[56] for twin boundaries cracking.

The missing of Stage II type fatigue crack propagation is another interesting observation in this study. There are some conditions favoring stage I crack propagation.[54] Low stresses resulting in slow growth favor stage I behavior. This can not be the only reason since stage II fatigue crack propagation has not been observed even for the highest strain

amplitude tests. The single slip orientation of the crystals certainly makes stage II fatigue crack propagation more difficult, but it is believed that local solute disordering which accompanies the deformation also plays an important role.

The scanning electron fractographs revealed another unusual fracture characteristic of both fully ordered and disordered crystals. The stage II fatigue striations have been observed on stage I fracture surfaces, as shown in Figure 21. Additional evidence is given in Figure 28, which shows both a "shear type" stage I fracture surface and stage II fatigue striations on a slanted surface. The result is rather surprising because some workers believe that it is mechanistically impossible to produce fatigue striations on slanted fracture surfaces.[27]

Several models have proposed for the formation of ductile fatigue striations.[53,54,57-59] Laird[53] suggests that a fatigue crack propagates by plastic blunting of the crack tip during the tensile part of the cycle followed by resharpening of the tip during the compression part of the cycle. However, Meyn[58] has shown that fatigue striations are not formed when the fatigue crack propagation test is performed in vacuum. This observation certainly challenges the validity of the plastic blunting theory for the formation of striations.

To explain the present results, a model based on slip-plane decohesion is suggested. This model has been put forward by Pelloux[59] and later by Broek,[60] and is based on the premise that under the tensile load the crack grows as a geometric consequence of slip displacements on two active slip systems. A second consequence of the slip displacements is crack tip blunting. Slip can proceed either alternately on one system and

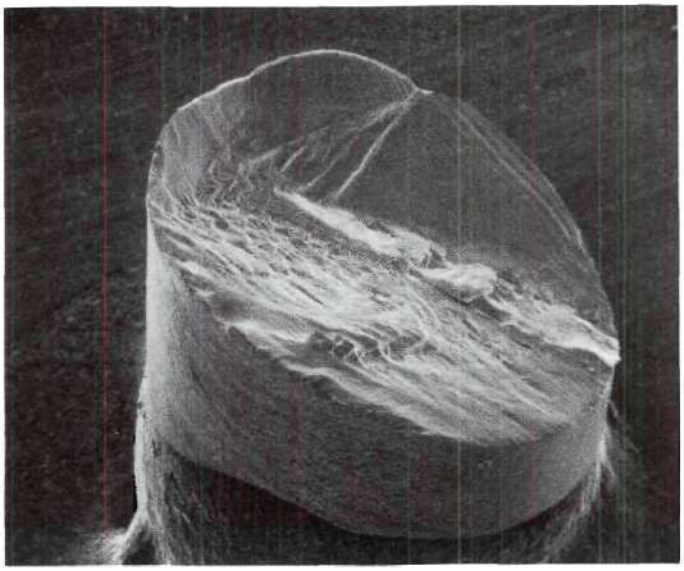

(a)

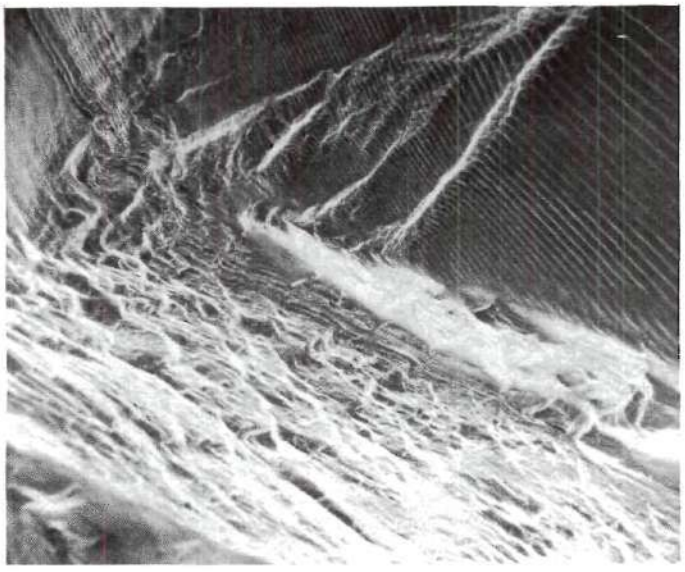

(b)

Figure 28. Scanning Electron Fractographs of Disordered Specimen Showing Both "Shear Fracture" and Fatigue Striations on Slanted Surface. ((a) and (b) show same area with different magnification, $\Delta\gamma_t/2 = \pm 1.65\%$, $N_f = 1800$ Cycles, (a) Magnification 24X, (b) Magnification 62X)

then on the other or simultaneously in both systems. During the compressive load, slip should take place in the opposite direction, at least in theory. However, in practice, the fact that the freshly exposed crack surface for most metals is immediately oxidized in air will limit the amount of reversibility of slip at the crack tip, and the fatigue striation is formed. For the elastic case and randomly oriented grains, it has been shown that the differences in resolved shear stresses on the various slip systems are small.[60] Probably the differences are small also in the plastic case. Under this condition of symmetric slip, the crack will grow on the bisecting plane of the two active slip planes, which is a direction approximately perpendicular to the stress axis. If the two slip systems contribute unequal amounts of slip, which is usually the case for a single crystal oriented for single slip, the crack will deviate from the bisecting plane to a plane which has the higher resolved shear stress. This explains the formation of fatigue striations on slanted fracture surfaces.

The scanning electron fractographs revealed that ordering has little effect on the fracture mode. As can be seen in Figures 19 and 20, both fully ordered and disordered crystals show ductile fracture. The reason for this can be explained in the following way. During the process of fatigue, the ordered structure is totally destroyed at the tip of fatigue crack due to the high plastic strain and this results in the same fracture mode for fully ordered and disordered crystals. X-ray scans of the fracture surfaces of the initially fully ordered samples failed to reveal any superlattice reflections, substantiating this view. The result is consistent with previous work that order generally leads to a moderate reduction in ductility with no change in fracture mode for f.c.c. materials.[1]

# CHAPTER VI

## CONCLUSIONS

1. Fully ordered $Cu_3Au$ single crystals exhibited an initial rapid fatigue hardening followed by fatigue softening. The rate of hardening or softening increases with increasing strain amplitude.

2. Disordered $Cu_3Au$ single crystals exhibited continuous fatigue hardening until fracture. The hardening rate increases with increasing strain amplitude and is low when compared to those in the initial stage of fully ordered crystals.

3. Fatigue hardening is interpreted by the application of unidirectional hardening concepts and softening by disordering.

4. The Manson-Coffin low cycle fatigue law is a good approximation of the low cycle fatigue behavior of $Cu_3Au$ single crystals both in fully ordered and disordered state.

5. At very high strain amplitudes, the low cycle fatigue resistance of the disordered crystals is superior over the ordered crystals by its higher fatigue ductility coefficient. As the strain amplitude decreases, the ordered crystals become increasingly stronger than the disordered crystals by their higher fatigue ductility exponents.

6. For both fully ordered and disordered crystals, the cyclic stress-strain curves are above the monotonic stress-strain curves. The fully ordered crystals cyclically harden much more than the disordered crystals.

7. For both fully ordered and disordered crystals, deformation bands develop during fatigue hardening for all strain amplitudes investigated. Deformation-band cracking becomes the predominant factor in the fracturing process.

8. For both fully ordered and disordered crystals, fatigue cracks were observed to nucleate at the intersection of primary slip bands and deformation bands and then propagated along the deformation band boundaries.

9. Ordering has little effect on the fracture mode, both fully ordered and disordered crystals show ductile fractures.

# BIBLIOGRAPHY


1. N. S. Stoloff and R. G. Davies, Progress in Materials Science, Vol. 13, Pergamon Press, New York (1966).

2. R. C. Boettner, N. S. Stoloff, and R. G. Davies, Trans. TSM-AIME, Vol. 236 (1966), p. 131.

3. R. S. Whitehead and F. W. Noble, J. Mater. Sci., Vol. 5 (1970), p. 851.

4. G. Rudolph, P. Haasen, B. L. Mordike, and P. Neumann, Proc. Ist. Internat. Cof. Fracture (Sendai, Japan), Vol. II (1965), p. 501.

5. J. C. Grosskreutz, Phys. Stat. Sol. (b), Vol. 47 (1971), p. 11.

6. B. E. Warren, "X-Ray Diffraction," Addison-Wesley Publishing Co., Reading, Mass. (1969).

7. G. Sachs and J. Weerts, Z. Phys., Vol. 67 (1931), p. 507.

8. G. W. Ardley, Acta Met., Vol. 3, Nov. (1955), p. 525.

9. J. S. Koehler and F. Seitz, J. Appl. Mechanics, Vol. 14 (1947), p. A217.

10. M. J. Marcinkowski, N. Brown, and R. M. Fisher, Acta Met., Vol. 9 (1961), p. 129.

11. R. G. Davies and N. S. Stoloff, Phil. Mag., Vol. 9 (1964), p. 349.

12. B. H. Kear, Acta Met., Vol. 12 (1964), p. 555.

13. P. A. Flinn, Trans. TSM-AIME, Vol. 218, Feb. (1960), p. 145.

14. A. E. Vidoz and L. M. Brown, Phil. Mag., Vol. 7 (1962), p. 1167.

15. R. G. Davies and N. S. Stoloff, Phil. Mag., Vol. 12 (1965), p. 297.

16. J. Czernichow and M. J. Marcinkowski, Met. Trans., Vol. 2, Nov. (1971), p. 3217.

17. S. B. Chakrabortty, Ph.D. Thesis (1974), Georgia Institute of Technology.

18. P. A. Flinn, G. M. McManus and J. A. Rayne, J. Phys. Chem. Solids, Vol. 15 (1960), p. 189.

BIBLIOGRAPHY (Continued)

19. D. E. Mikkola and J. B. Cohen, Acta Met., Vol. 14, Feb. (1966), p. 105.

20. K. Salama, F. Shaikh, and J. M. Roberts, Acta Met., Vol. 19, May (1971), p. 395.

21. D. R. Chipman, J. Appl. Phys., Vol. 27 (1965), p. 739.

22. C. K. H. DuBose and J. O. Stiegler, Oak Ridge National Laboratory, Contract No. W-7405-eng-26, Feb. (1967).

23. R. M. Fisher and M. J. Marcinkowski, Phil. Mag., Vol. 6 (1961), p. 1385.

24. JoDean Morrow, ASTM STP 378 (1965), p. 45.

25. R. W. Landgraf, ASTM STP 467 (1970), p. 3.

26. R. Maddin and N. K. Chen, Progress in Metal Physics, Vol. 5, No. 2 (1954), p. 53.

27. D. A. Ryder, "The Elements of Fractography," University of Manchester, Institute of Science & Technology, Manchester, England (1971), p. 127.

28. W. G. Johnston and J. Gilman, J. Appl. Phys., Vol. 31 (1960), p. 632.

29. A. S. Tetelman, Acta Met., Vol. 10 (1962), p. 813.

30. C. E. Feltner and C. Laird, Acta Met., Vol. 15, No. 10, Oct. (1967), p. 1633.

31. B. H. Kear, Acta Met., Vol. 14, May (1966), p. 659.

32. C. E. Feltner and C. Laird, Acta Met., Vol. 15, No. 10, Oct. (1967), p. 1621.

33. N. J. Wadsworth, Acta Met., Vol. 11, No. 7, July (1963), p. 663.

34. A. H. Cottrell, "Relation of Properties to Microstructure," Cleveland, Ohio (Amer. Soc. Metals) (1954), p. 131.

35. J. C. Grosskreutz, Met. Trans., Vol. 3, May (1972), p. 1255.

36. C. Calabrese and C. Laird, Mater. Sci. Eng., Vol. 13 (1974), p. 141.

37. J. B. Cohen, "A Brief Review of the Properties of Ordered Alloys," Northwestern University (1970).

BIBLIOGRAPHY (Continued)


38. M. J. Marcinkowski, "Electron Microscopy and Strength of Crystals," edited by Gareth Thomas & Jack Washburn, 1963 Interscience Publishers, p. 333.

39. J. M. Cowley, J. Appl. Phys., Vol. 21 (1950), p. 24.

40. R. W. Cahn, "Local Atomic Arrangements Studied by X-Ray Diffraction," Girdon and Breach, New York (1966).

41. J. C. Fisher, Acta Met., Vol. 2, Jan. (1954), p. 9.

42. J. R. Hancock and J. C. Grosskreutz, Acta Met., Vol. 17, Feb. (1969), p. 77.

43. D. T. Raske and JoDean Morrow, ASTM STP 465 (1969), p. 1.

44. L. F. Coffin, Jr., TASMA, Vol. 76 (1954), p. 931.

45. S. S. Manson, Machine Design, MADEA, Nov. 23 (1961), p. 165.

46. R. K. Ham, Canad. Met. Quart., Vol. 5, No. 3 (1966), p. 161.

47. R. K. Ham, The Institute of Metals, No. 32 (1967), p. 55.

48. C. E. Feltner and P. Beardmore, ASTM STP 467 (1970), p. 77.

49. J. A. Collins and C. H. Mathewson, Trans. AIMME, Vol. 137 (1940), p. 150.

50. N. K. Chen and C. H. Mathewson, Trans. AIMME, Vol. 191 (1951), p. 653.

51. M. Doner, J. C. Diprimio, and E. I. Salkovitz, Acta Met., Vol. 21, Nov. (1973), p. 1547.

52. G. Y. Chin and W. A. Backofen, J. Inst. Metals, Vol. 90 (1961), p. 13.

53. C. Laird, ASTM STP 415 (1967), p. 131.

54. P. J. E. Forsyth, Proceedings of The Crack Propagation Symposium, Cranfield, England, Vol. 1, Sept. (1961), p. 76.

55. J. R. Low, Jr., Met. Soc. Conf., Vol. 20 (1963), p. 197.

56. D. Hull, J. Inst. Metals, Vol. 86 (1957), p. 425.

BIBLIOGRAPHY (Concluded)

57. R. W. Hertzberg, ASTM STP 415 (1967), p. 205.

58. D. A. Meyn, Trans. ASM, Vol. 61, March (1968), p. 42.

59. R. M. N. Pelloux, Trans. ASM, Vol. 62 (1969), p. 281.

60. D. Broek, "Some Contributions of Electron Fractography to the Theory of Fracture," NLR TR 72029 U.

# VITA

Kuang-Ho Chien, the son of Mr. and Mrs. S. Y. Chien, was born in Taipei, Taiwan on March 10, 1938. He graduated from Cheng-Kung University, Taiwan and received a Bachelor's degree in Metallurgical Engineering there in June, 1960.

He entered Tatung Engineering Co., Taiwan as a metallurgical engineer in March, 1962. In January, 1969 he came to the United States and entered the University of Connecticut, Storrs, Connecticut, where he received a Master of Science in Metallurgy in June, 1970. In September, 1971 he came to the Graduate Division of the Georgia Institute of Technology.

He married the former Joan Miau-Jen Kao of Taipei, Taiwan in December, 1971.